1   **Mutations in *ACTL6B* cause neurodevelopmental deficits and epilepsy and lead to**

2   **loss of dendrites in human neurons**

3

4   Scott Bell [1,34], Justine Rousseau [2,34], Huashan Peng[1], Zahia Aouabed[1], Pierre Priam[3],

5   Jean-Francois Theroux[1], Malvin Jefri[1], Arnaud Tanti[1], Hanrong Wu[1], Ilaria Kolobova[1],

6   Heika Silviera[1], Karla Manzano-Vargas[1], Sophie Ehresmann[2], Fadi F Hamdan[1], Nuwan

7   Hettige[1], Xin Zhang [1], Lilit Antonyan[1], Christina Nassif[4], Lina Ghaloul-Gonzalez[4],

8   Jessica Sebastian[5], Jerry Vockley[5], Amber G. Begtrup[6], Ingrid M. Wentzensen[6], Amy

9   Crunk[6], Robert D. Nicholls[7], Kristin C Herman[7], Joshua Deignan[8], Walla Al-Hertani[9],

10   Stephanie Efthymiou[10], Vincenzo Salpietro[10], Noriko Miyake[11], Yoshio Makita[11],

11   Naomichi Matsumoto[12], Rune Østern[13], Gunnar Houge[14], Maria Hafström[13], Emily

12   Fassi[15], Henry Houlden[16], Jolien S Klein Wassink-Ruiter[17], Dominic Nelson[18], Amy

13   Goldstein[19], Tabib Dabir[20], Julien van Gils[21], Thomas Bourgeron[21], Richard Delorme[22],

14   Gregory M Cooper[23], Jose E. Martinez[24], Candice R Finnila[25], Lionel Carmant[24], Anne

15   Lortie[25], Renske Oegema[26], Koen van de Gassen[26], Sarju G. Mehta[27], Dagmar Huhle[27],

16   Rami Abou Jamra[28], Sonja Martin[29], Han Brunner[30], Dick Lindhout[31], Margaret Au[32],

17   John M Graham Jr[32], Christine Coubes[33], Gustavo Turecki[1], Simon Gravel[17], Naguib

18   Mechawar[1], Elsa Rossignol[2], Jacques L Michaud[2], Julie Lessard[3], Carl Ernst [1,34,*],

19   Philippe M Campeau [2,34,*]

20

21   **Affiliations**

22

23   1) Psychiatric Genetics Group, Douglas Hospital Research Institute, McGill University,
24   Montreal, QC, Canada, H4H 1R3
25   2) CHU-Sainte Justine Research Centre, University of Montreal, Montreal, QC, Canada,
26   H3T 1C5,
27   3) Institute for Research in Immunology and Cancer (IRIC), University of Montreal,
28   Montreal, Quebec, Canada, H3T 1J4

29 4) Department of Pediatrics, University of Pittsburgh, Children's Hospital of Pittsburgh of
30 UPMC, Pittsburgh, PA, USA
31 5) Division of Medical Genetics, University of Pittsburgh, Children's Hospital of
32 Pittsburgh of UPMC, Pittsburgh, PA, USA
33 6) Gene Dx, Gaithersburg, MD 20877, USA
34 7)University of California at Davis Medical Center, Section of Medical Genomics,
35 Sacramento, CA, USA 95817
36 8) Department of Pathology and Laboratory Medicine, David Geffen School of Medicine
37 at UCLA, CA, USA
38 9) Departments of Medical Genetics and Paediatrics, Cumming School of Medicine,
39 Alberta Children's Hospital and University of Calgary, Calgary, AB T3B 6A8
40 10) Department of Molecular Neuroscience, UCL Institute of Neurology, Queen Square
41 WC1N 3BG, London, UK
42 11) Department of Human Genetics, Yokohama City University Graduate School of
43 Medicine, Yokohama 236-0004,Japan
44 12) Education Center, Asahikawa Medical University, Asahikawa 078-8510, Japan,
45 13) Department of Medical Genetics, St. Olavs hospital, Trondheim University Hospital,
46 Postbox 3250 Sluppen, NO-7006 Trondheim
47 14) Center for Medical Genetics and Molecular Medicine, Haukeland University Hospital,
48 5021 Bergen, Norway
49 15) Division of Genetics and Genomic Medicine, Department of Pediatrics, Washington
50 University School of Medicine, St. Louis, MO, USA, 63110
51 16) Department of Molecular Neuroscience, UCL Institute of Neurology, Queen Square
52 WC1N 3BG, London, UK
53 17) Department of Genetics, University of Groningen and University Medical Center
54 Groningen, 9700 RB Groningen, the Netherlands
55 18) McGill University, Department of Human Genetics, Montreal, QC, H3G 0B1
56 19) Division of Child Neurology, Children's Hospital of Pittsburgh, Pittsburgh,
57 Pennsylvania, USA.
58 20) Northern Ireland Regional Genetics Centre, Belfast Health and Social Care Trust,
59 Belfast City Hospital, Lisburn Road, Belfast BT9 7AB, UK
60 21) Human Genetics and Cognitive Functions, Institut Pasteur,, 25 Rue du Docteur
61 Roux, Paris, Cedex 15 France
62 22) Assistance Publique Hôpitaux de Paris (APHP), Robert Debré Hospital, Child and
63 Adolescent Psychiatry Department, Paris, France
64 23) HudsonAlpha Institute for Biotechnology, Huntsville, AL 35806
65 24) Children's Rehabilitation Service, Mobile, AL 36604
66 25) Department of Neurology, University of Montreal, Montreal, Canada
67 26) Department of Genetics, University Medical Center Utrecht, 3508 AB Utrecht, the
68 Netherlands.
69 27) Department of Clinical Genetics, Addenbrookes Hospital, Cambridge CB2 0QQ
70 28) Institute of Human Genetics, University Medical Center Leipzig, 04103 Leipzig,
71 Germany
72 29) Department of Human Genetics, Radboud University Medical Center, Donders
73 Institute for Brain, Cognition and Behaviour, Nijmegen, 6500 GA, The Netherlands.
74 30) Department of Clinical Genetics and School for Oncology & Developmental Biology
75 (GROW), Maastricht University Medical Center, 6202 AZ, Maastricht, The Netherlands.
76 31) Department of Genetics, University Medical Center Utrecht, Utrecht & Stichting
77 Epilepsie Instellingen Nederland (SEIN), Heemstede, The Netherlands.
78 32) Medical Genetics, Cedars Sinai Medical Center, Los Angeles CA 90048 USA

79   33) Service de génétique clinique, Département de génétique médicale, Maladies rares
80   et médecine personnalisée, Centre de Référence Anomalies du développement et
81   Syndromes malformatifs du Sud-Ouest Occitanie Réunion, CHU de Montpellier, 34295
82   Montpellier cedex 5, France
83   34) Equally contributing authors
84

85   *Corresponding authors: carl.ernst@mcgill.ca; p.campeau@umontreal.ca

86   Running title (40 characters): Mutations in *ACTL6B* cause neurodevelopmental disorders

89

90

91

92

Abstract

We identified individuals with mutations in ACTL6B, a component of the chromatin

remodelling machinery including the BAF complex. Ten individuals harbored bi-allelic

mutations and presented with global developmental delay, epileptic encephalopathy and

spasticity, and ten individuals with de novo heterozygous mutations displayed intellectual

disability, ambulation deficits, severe language impairment, hypotonia, Rett-like

stereotypies and minor facial dysmorphisms (wide mouth, diastema, bulbous nose). Nine

of these ten unrelated individuals had the identical de novo c.1027G>A mutation. Human

derived neurons were generated that recaptured *ACTL6B* expression patterns in

development from progenitor cell to post-mitotic neuron, validating the use of this cell

model. Engineered knock-out of *ACTL6B* in wildtype human neurons resulted in

profound deficits in dendrite development, a result recapitulated in two individuals with

different bi-allelic mutations, and reversed on clonal genetic repair or exogenous

expression of *ACTL6B*. Whole transcriptome analyses and whole genomic profiling of

the BAF complex in wildtype and biallelic mutant *ACTL6B* NPCs and neurons revealed

increased genomic binding of the BAF complex in *ACTL6B* mutant cells, with

corresponding transcriptional changes in several genes including *TPPP* and *FSCN1*,

suggesting that altered regulation of some cytoskeletal genes contribute to altered

dendrite development. Assessment of bialleic and heterozygous *ACTL6B* mutations on

an *ACTL6B* KO human background demonstrated that biallelic mutations mimic

engineered deletion deficits while heterozygous mutations do not, suggesting that the

former are loss-of-function and the latter are gain-of function. These results reveal a role

for *ACTL6B* in neurodevelopment, and implicate another component of chromatin

remodelling machinery in brain disease.

Introduction

118

119   *ACTL6B* (MIM: 612458) encodes an actin-related protein (ARP), which are a

120   class of proteins that resemble actin and have roles in chromatin remodelling and

121   histone acetylation[1]. Though ACTL6B, known as BAF53B, may interact with multiple

122   complexes in a particular spatiotemporal order, most investigations have focused on its

123   role in the BAF (BRG1/BRM-Associated Factor), or SWI/SNF complex[2], which serves as

124   an important regulator of gene expression by remodeling nucleosomes in an ATP-

125   dependant fashion[3-5]. In order to regulate different sets of genes during development,

126   BAF subunits can be exchanged with homologous alternatives[3]. One such switch in BAF

127   subunit composition occurs in developing neural cells as they exit the cell cycle. During

128   this time, the neural progenitor specific BAF (npBAF) complex transitions to the neural

129   specific BAF (nBAF) complex through the exchange of several subunits, including

130   BAF53A for its paralog BAF53B[6]. This is partly achieved through increased expression

131   of miR-9* and miR-124 in post mitotic neurons, which repress the expression of the gene

132   that encodes BAF53A, *ACTL6A* (MIM: 604958)[7]. nBAF complexes can bind the

133   transactivator CREST and be recruited to genes crucial for dendritogenesis through

134   interactions mediated by BAF53B[8]. As a result, loss of BAF53B protein levels during

135   neuronal development results in impaired dendritic outgrowth. An *Actl6b* KO mouse has

136   previously been generated, and found to have deficits in dendritic spine and synapse

137   function, leading to impaired long-term memory and poor survival[9].

138   While different genes that contribute to the BAF complex have been found to be

139   associated with human disease (e.g., Nicolaides-Baraitser syndrome MIM: 601358,

140   *SMARCA2* MIM:600014; Coffin-Siris syndrome MIM: 135900, *ARID1B; MIM:* 614556)[10;

141   [11], *ACTL6B* has not been conclusively reported to have a deleterious role in human

142   neurological diseases. In this study, we identified individuals with neurodevelopmental

5

143 disorders with either inherited recessive mutations or dominantly acting *de novo*

144 mutations in *ACTL6B*, and sought to understand how mutations in *ACTL6B* might affect

145 the development of human neurons.

146

Materials and methods

Description of studied individuals. Individuals had whole exome sequencing as part of local neurodevelopmental studies on developmental delay and intellectual disability, autism or epilepsy (R1, R2a/b, R3a/b, R4, R5, R7, R9, R10, D2, D3, D7, D8). Informed consent for participating in the genetic studies was obtained on protocols approved by institutional review boards of local hospitals. Individuals D1 and D4 were enrolled in the DDD study and provided informed consent for this study. Other individuals had exome sequencing at GeneDx as part of clinical care (individuals R6, R8a/b, D5, D6, D9), and after *ACTL6B* was identified as a candidate gene, provided informed consent for the sharing of photographs or samples as applicable.

Experimental procedures for sequencing. DNA was extracted from peripheral blood from affected individuals and parents using standard protocols. For individuals who had Whole Genome Sequencing (R1, R2a/b, R10), the DNA libraries were prepared by using the Illumina TruSeq DNA PCR-Free kits using the manufacturer's protocol. For individuals who had Whole Exome Sequencing, the exome libraries were prepared using Agilent SureSelect kits (R3ab, R4, R6, R8ab, R9, D1, D2, D4-D9), Roche-NimbleGen EZ exome kits (R5, D3) and Illumina Nextera kits (R7). More details included in Tables 1 and 2. All libraries were then sequencing on Illumina HiSeq systems.

Analysis of sequencing data. Sequences were aligned using BWA, GATK, Novoalign, Isaac, or LifeScope software. The variants were called using GATK, SAMtools, Annovar, CarpeNovo, Isaac, LifeScope and in-house pipelines. More details can be found in Tables S1 and S2. After identification of candidate variants in *ACTL6B*, their segregation was confirmed by Sanger sequencing using standard protocols.

172 **Fibroblast reprogramming to induced pluripotent stem cells (iPSCs)** Fibroblasts

173 were obtained from biopsies or from Coriell (Table S3), and cultured in DMEM

174 (Invitrogen) supplemented with 10% bovine serum albumin (Invitrogen). Fibroblasts

175 were reprogrammed using episomal reprogramming vectors containing Oct4, Sox2,

176 Myc3/4, Klf4, ShRNA P53 (ALSTEM) and a puromycin resistance gene using a Neon

177 Transfection System (Invitrogen). Following transfection, cells were plated on tissue

178 culture plates coated with Matrigel (Corning) in TesR-E7 media (Stem Cell

179 Technologies) supplemented with 2ug/ml puromycin (Sigma). Following 48hrs of

180 puromycin selection, fresh TesR-E7 media was exchanged, until distinct and robust

181 iPSC colonies formed, at which point mTESR1 media (Stem Cell Technologies) was

182 used to maintain and proliferate the colonies.   Quality control experiments for iPSCs

183 include mycoplasma testing, short tandem repeat profiling to ensure no sample mix-ups,

184 assessment of endogenous pluripotency factor, immunocytochemistry for pluripotency

185 markers, and molecular karyotyping.

186

187 **Molecular Karyotyping** To ensure no chromosomal abnormalities occurred as a result

188 of iPSC induction or gene editing, DNA from all generated iPSC lines was sent to Prince

189 of Wales Hospital (Shatin, Hong Kong) for sequencing on an Ion Torrent Hi-

190 Q Sequencer (Thermofisher). Samples were sequenced with an average of 4 million

191 150bp reads per sample, for an average coverage of 0.0014X. Analysis was preformed

192 using CNV-Seq[12].   Positive controls included cells of origin and cells from families with

193 first-degree relationships where we could detect Mendelian inheritance of CNVs >1Mb.

194

Differentiation of iPSCs to forebrain neural progenitor cells (NPCs) iPSCs were differentiated to forebrain NPCs according to our previously described methods [13; 14]. iPSC colonies were dissociated and resuspended in DMEM/F12 media supplemented with N2 (Invitrogen) B27 (Invitrogen),and BSA [1 mg/ml], Y27632 [10 µM] (AdooQ Bioscience), SB431542 [10 mM](Selleckchem), and Noggin [200 ng/ml](GenScript), onto non-adherent plates to form organoids. After one week of maintenance as organoids, cells were dissociated and plated on Matrigel coated plates in DMEM/F12 supplemented with B27, bFGF (20ng/ml), EGF (20ng/ml), and laminin[1ug/ml] for a further seven days of differentiation, with media exchanged every three days. Cells were assessed for NPC morphology, and stained for markers of forebrain NPCs (PAX6, SOX2, TUJ1) and OCT4.

Differentiation of NPCs to Post-mitotic Neurons For short term (5 days) differentiation, NPCs were plated in DMEM/F12 media supplemented solely with B27. If longer term (>5 days) differentiation was required, NPCs, were plated in BrainPhys SM1 (Stem Cell Technologies) and N2-A supplemented media (Stem Cell Technologies). 50% of this media was exchanged every three days. Previous work has shown that neurons generated using this methodology express both GABAergic (~30%) and Glutamatergic (60%) markers[14] and are negative for midbrain markers, such as tyrosine hydroxylase. Approximately 5-10% of cells stain for GFAP, an astrocyte marker.

Whole Cell Recordings For whole-cell patch-clamp recordings, individual coverslips containing differentiated hIPSC-Derived Neurons were transferred into a heated recording chamber and continuously perfused (1 ml/min) with BrainPhys™ Neuronal

Medium (Catalog # 05791; StemCell Technologies) bubbled with a mixture of CO_2 (5%) and O_2 (95%) and maintained at 25 °C. Whole-cell patch clamp recordings were obtained using borosilicate pipettes (3–6 MΩ), filled with intracellular solution that contained the following (in mM): 5 HEPES, 2 KCl, 136 potassium gluconate, 5 EGTA, 5 Mg-ATP, 8 creatine phosphate, and 0.35 GTP. The pH was adjusted to 7.27 with KOH, and the osmolarity adjusted with distilled water or concentrated potassium gluconate if needed to between 295 and 298 mOsm with an osmometer (3320; Advanced Instruments). After a recording was completed, the nominal membrane potential in voltage- and current-clamp recordings was corrected for the calculated 10 mV liquid junction potential. All potential values reported reflect this correction. Once whole-cell recording had been established, neurons were routinely held in voltage clamp at -70 mV except when examining changes in the resting membrane potential and rheobase, which was performed in current clamp. Cells were only studied if they exhibited a stable holding current and access resistance for at least 10 min before experimental manipulations. Data were acquired using a Digidata 1550A/ Multiclamp 700B (Axon Instruments) and Clampex 10.5 (Molecular devices). Currents were filtered at 2 kHz and digitized at 20 kHz.

CRISPR/Cas9 gene editing A double nickase CRISPR/Cas9 gene editing system with a Paprika RFP (pRFP) reporter and gRNA targeting the first exon of the *ACTL6B* was used for KO experiments. For ACTL6Bext33 repair experiments, a wild-type CRISPR/CAS9-pRFP gene editing system was used to target the mutation in the stop codon of exon 14 of *ACTL6B*. One µg of construct was added per transfection reaction, and transfection was carried out simultaneously with iPSC induction to ensure clonality, as previously described[14]. Following transfection, cells were selected for puromycin

244 resistance and RFP visualization as described[8] allowing for cell expansion from a single

245 edited fibroblast. Potentially edited colonies were expanded and stored as cell lines after

246 which DNA was extracted and Sanger sequenced at Genome Quebec.

247

248 **RNA Sequencing** RNA samples with RIN values >9.0 were submitted to Genome

249 Quebec for RNA sequencing. Eight libraries were run per lane of an Illumina HiSeqV4

250 2500 flow cell (125 bp paired-end reads), which achieved an average of ~40 million

251 reads per library. For bioinformatic processing, we used FASTX-Toolkit, TopHat[15]

252 Bowtie2[16], and Cufflinks2[17] with default parameters to preprocess, align, and assemble

253 reads into transcripts, estimate abundance, and test differential expression.   More

254 detailed methods can be found here[18].

255

256 **Western Blot** Cells were lysed with RIPA buffer (Sigma) supplemented with

257 SIGMAFAST™ Protease Inhibitor Tablets (Millipore-Sigma). Protein concentrations were

258 determined using a Pierce BCA Protein Assay Kit (ThermoFisher). Approximately 15 µg

259 of protein was loaded per well in Mini-PROTEAN® TGX Stain-Free™ Precast Gels

260 (Biorad). Gels were run at 150V for approximately 75 minutes, and then transferred to a

261 nitrocellulose membrane using a Trans-Blot® Turbo™ Transfer System (Biorad).

262 Membranes were blocked in 4% non-fat milk dissolved in TBS-T buffer (tris-buffered

263 saline-tritonX; Sigma-Aldrich) for twenty minutes, and then incubated with primary

264 antibodies overnight at 4^0C with shaking. Blots were washed three times in TBS-T for

265 five minutes, and then incubated with appropriate mouse or rabbit secondary antibodies

266 for one hour at room temperature. Blots were washed a further three times in TBST for

267 five minutes, then imaged using a ChemiDoc™ XRS+ System (Biorad). Blots were

268 imaged and analysed using ImageLab (Biorad) software, and statistical analysis was

269   preformed using student T-tests when two samples conditions were present and a one-

270   way ANOVA when more than two sample conditions were present. Blots were

271   normalized to β-actin. Further details on the antibodies used for WB can be found in

272   Table S5.

273

274   **Quantitative PCR** Reverse transcriptions were done on the total RNA fraction in order to

275   obtain cDNA in 40 µl volume containing 1 µg of total RNA, 0,5 µg random primers, 0.5

276   mM dNTPs, 0,01 M DTT and 400 U M-MLV RT (Invitrogen). The reactions were

277   performed in a total volume of 20µl volume on a 384 well plate either using an Applied

278   Biosystems 7900 HT (Applied Biosystems) or a QuantStudio 6 (Thermofisher) PCR

279   Machines. For each well, PCR mix included 10µl of Power SybrGreen PCR Mastermix

280   (Life Technologies), 1 µl of primers/probe mix, 2 µl of cDNA, H20 up to 20 µl. Serial

281   dilutions of a mix of cDNA ranging between 0.003052 ng and 50 ng were used to

282   generate a calibration curve for an absolute quantification. Protein levels were given as a

283   ratio between the relative quantities of the gene of interest and the endogenous control.

284   GAPDH was used as internal control for normalization. The normalized expression levels

285   were then compared between cell lines using either a student's t-test or an ANOVA with

286   post-hoc t-test. Further details on the primers used for qPCR can be found in Table S6.

287

288   **Immunofluorescence**   Adherent Cells were washed with PBS, then fixed with 3%

289   paraformaldehyde (Sigma-Aldrich) on slides for fifteen minutes. Samples were

290   permeabilized with 0.5% TX-100 (Sigma-Aldrich) in 0.5% PBS-BSA for fifteen minutes,

291   and then blocked in 0.5% PBS-BSA for an additional fifteen minutes. Primary antibodies

292   were added in appropriate dilutions (Table S5) in 0.5% PBS-BSA and added to samples

293   for 30 minutes.   Samples were washed in 0.5% PBS-BSA containing an appropriate

294   dilution of secondary antibody (Table S5) was added to the samples and incubated for

295   thirty minutes in the dark. Samples were washed with 0.5% PBS-BSA. Samples were

296   then visualized on an Apotome Florescent microscope (Zeiss). Neurolucida Tracing

297   Software (MBF Bioscience) was used to measure nuclei surface area, soma surface

298   area, and projection length. Images were processed and scale bars added in Image J.

299

300   **Chromatin immunoprecipitation (ChIP) sequencing**   Samples were prepared for

301   CHiP-Seq and CHiP-qPCR using a Magna ChIP-Seq™ kit (Millipore-Sigma). Cells were

302   cross linked at day 0 and day 5 of differentiation by immersion in 37% formaldehyde.

303   Glycine was added at a final concentration of 125uM to the samples to inactive cross-

304   linking. DNA was sheared using a S220 Sonicator (Covaris), and precleared using a

305   protein A or G agarose beads. All samples were then probed using both a mouse

306   monoclonal (Santa Cruz, sc-17796) and rabbit polyclonal (Santa Cruz, sc-10768)

307   antibody directed against BRG1 overnight at 4^0C. A IGG control was ran for both rabbit

308   polyclonal and mouse monoclonal antibodies using a pooled sample composed of equal

309   parts of all samples used for CHiP. A 0.2M glycine solution pH 2.6 was used for elution

310   of cross-linked proteins and DNA from the beads. DNA was purified using Agencourt®

311   AMPure® XP Beads (Beckman Coulter). Libraries were constructed using an NGS

312   Library Preparation Kit (Millipore-Sigma) and sent to Genome Quebec, where they were

313   sequenced using a Illumina HiSeqV4 2500 flow cell (125 bp paired-end reads) with

314   between 11-12 samples sequenced per lane.

315   **ChIPSeq Analysis**

316   ***Quality trimming and pre-processing***   Sequencing adaptors were clipped using Trim

317   Galore. Quality trimming was done with same tool. A phred score cut-off value of 20 was

318   used. Reads shorter than 20bp were filtered out. Reads were aligned to the Human

319   Reference Genome (hg19) using BWA software version 0.7.10. Resulting bam files

320   were filtered for minimal mapping quality (MAPQ ≥ 20) and all alignments with samflag 4

321   (read unmapped) were excluded using SAMtools (version 0.1.19). Duplicates reads were

322   removed using the MarkDuplicates module of Picard (version 1.141) with the option

323   REMOVE_DUPLICATES=true.

324

325   **_Peak calling_** The identification of ChIP-seq enriched regions (peaks) was performed

326   using MACS2 (version 2.1.1); (macs2 callpeak --format BAM --broad --nomodel -q 0.05

327   --broad-cutoff 0.1 --extsize 500). Differential binding-sites analysis were done using the

328   DiffBind Bioconductor R package (version 2.6.6)[4]. Diffbind calls some of the DESeq2

329   (version 1.18.1) functions to perform the contrast analysis between pairwise

330   p.*427Aspext*33 or Control D5 vs D0 groups (dba.analyze (method = DBA_DESEQ2)).

331   For each comparison, DiffBind generated a set of consensus peaks with the requirement

332   that peaks must be in at least two of the samples (minOverlap = 2). Standardized

333   differential analysis was then performed using the following default settings for

334   dba.analyze: method=DBA_DESEQ2, FDR <= 0.05, bSubControl parameter set to

335   TRUE, bFullLibrarySize set to TRUE. Thus, raw number of reads in the control sample

336   was subtracted and the library size was computed for each sample and used for the

337   normalization. sizeFactors is called with the number of reads in the BAM files for each

338   ChIP sample, divided by the minimum of these. The final normalized counts returned are

339   the raw reads (adjusted for control reads) divided by the normalization factors (result of

340   calling sizeFactors()). Significantly different peaks were then annotated with HOMER

341   (version 4.7)[6] using RefSeq annotations (distal_distance = -10000, distance5d_lower

342   =-10000, distance5d_upper = -100000, gene_desert_size=100000, proximal_distance=-

343   2000).

344

345

Results

Identification of French Canadian families with homozygous mutations in *ACTL6B*

By exome sequencing of families with neurodevelopmental disorders in Quebec, we identified a family with two children with a homozygous mutation in *ACTL6B* that eliminates the stop codon (c.1279del, NM_016188.4) and extends the reading frame by an additional 33 amino acids (p.*427Aspext*33; NP_057272.1; Individual R3, Figure 1, Table 1, Table S1).

Sequencing both affected children, their unaffected older brother, and both parents from family R3 revealed that c.1279del was the only mutation identified in the family that was protein altering, followed an autosomal recessive inheritance model and was absent from all genomic databases. Both parents and the unaffected brother were carriers, and all are healthy. The phenotype of the disorder is severe: both brothers died early (4 and 6 years) of aspiration asphyxiation, were non-verbal, non-ambulatory, and required 24-hour care for all needs. Parents reported incessant crying (10+ hours per day), seizures beginning at 3 months, and sleep difficulties, (Table 1). An MRI of the brain was provided and had no indications from the reviewing radiologist. Careful tracing of the lineage of family R3 using Catholic Church records[7] revealed a common ancestor, which we determined to be the most likely origin of the mutation in Family R3 (Figure S1A and Supplemental Methods). We genotyped five other members from family R3 across four generations and could identify appropriate inheritance of the mutation from the predicted founder (Figure S1B). The R3 parents of the proband can be traced to a brother and sister going back six generations in the mother and five generations in the father, an event unknown to the R3 parents prior to birth of the probands (Figure S1B).

371   Another French Canadian family (defined as both great grandparents being born in the

372   province of Quebec, Canada) with child R10 (Table 1) also had this same mutation with

373   almost identical phenotype, suggesting that this mutation is not private to the R3 family

374   but rather may be a specific but rare variant in the French Canadian population. We

375   assume that these families are distantly related but could not identify the branch point at

376   which the pedigrees may overlap between families R3 and R10.

377

378   **Biallelic mutations in *ACTL6B* cause a severe neurodevelopmental disorder**

379   We were able to identify eight additional families with a similar phenotype (Table

380   1, Table S1) with biallelic mutations. A majority of these identified mutations resulted in

381   premature termination codons, and were located in highly conserved sequences (Figure

382   1B-C). We considered it very likely that most of these mutation sites resulted in

383   nonsense mediated decay (NMD) of the transcript, as they occur well in advance of the

384   penultimate exon[19], and strongly suggests that the disease is due to loss of function of

385   the *ACTL6B* gene. However, some mutations, including the c.1279del mutation were

386   located in the final exon of *ACTL6B* (Figure 1B), and were therefore not predicted to lead

387   to NMD[19]. Heterozygous stop mutations are present in healthy parents, suggesting a

388   recessive disorder. Selected case vignettes can be found in the Supplemental section.

389

390   **De novo missense mutations at specific loci in *ATCL6B* cause a different, severe**

391   **neurodevelopmental disorder**

392

393   Over the course of identifying subjects with mutations in *ACTL6B*, we found ten

394   individuals with heterozygous *de novo* missense mutations in *ACTL6B* with hypotonia,

395   intellectual disability, developmental delay, autism, and Rett-like stereotypies such as

396   handwringing (Figure 1, Table 2, Table S2). Detailed case vignettes of some subjects

397 are presented in the Supplemental section. This was surprising, given that we observed

398 heterozygous stop/Frameshift mutations in healthy individuals arguing for a recessive

399 inheritance model. Nine of ten of these individuals possess the same well conserved

400 c.1027G>A mutation (Figure 1C and Table 2). p.Gly343Arg (NM_016188.4,

401 HG19:chr7:100244258; Exon 12), is not seen in the 60,706 ExAC subjects. The same

402 holds true for the other observed variant, p.Asp77Gly (NM_016188.4; HG19: chr7:

403 100253082; exon 3), both of which are likely gain-of-function mutations since

404 heterozygous stop mutation carriers have no disease. 3D modeling of the *de novo*

405 dominant and the recessive biallelic mutations (Figure 1D) shows no spatial clustering of

406 mutation sites.BAF53B has an actin-related domain, which is subdivided into four

407 subdomains[20]. Subdomain I and III are structural, and also contain residues that interact

408 with ATP[21]. Subdomain II is the smallest domain, and enables the protein to have polar

409 and non-polar orientations. Previous work has shown that mutations in this subdomain

410 impair dendritic outgrowth[4]. Subdomain IV interacts with subdomain 1[20] and is

411 necessary for the interaction of the protein with actin[21]. We mapped these subdomains

412 onto a model of BAF53B derived from the S.cervisiae; ARP4 structure, and found that

413 the variants occurred in all subdomains. Specifically, p.Phe147del, p.Cys425,

414 p.Arg130Gln and p.Gln411* variants occur in Subdomain I, the p.Asp77Gly variant

415 occurred in Subdomain II, p.Gly343Arg, p.Gly349Ser and p.Arg130Gln occur in

416 Subdomain III, and p. Gly425*, occur in Subdomain IV (Table 1-2). We did not find any

417 concentration of mutations in a particular domain.

418

419   Two other BAFopathies, Nicolaides-Baraitser syndrome (MIM:600014) and

420 Coffin-Siris syndrome (MIM: 614556), so called because they affect genes that code for

421 proteins that can be incorporated into the BAF complex, have sparse scalp hair and

422   coarse facial features, though this is a wide spectrum in affected individuals. We

423   obtained images of several probands in this study and did not observe coarse features in

424   the majority of subjects (Figure 1A). However, in individuals with the dominant mutations,

425   we did find common features such as a wide mouth, diastema and bulbous tip of the

426   nose. In the case of MRI brain structure this was grossly normal, with subtle but not

427   specific features (common across many MRI scans of children with neurodevelopmental

428   diseases) detected for some individuals (Table S1, S2)).

429

430   **Modeling the p.*427Aspext*33 variant in human neurons**

431   Human stem cells are a powerful model for functional genetic studies as mutations can

432   be assayed on a relevant genetic background and are amenable to genetic engineering.

433   All iPSC lines generated in this study had normal chromosomal integrity, presented

434   typical hallmarks of pluripotency (Figure 2A), including expression of endogenous

435   pluripotency genes (Figure S2A-B), and had the capacity to differentiate into all three

436   germ layers (Figure S2C). iPSCs were utilized to generate forebrain neural progenitor

437   cells (NPCs), which expressed neural and forebrain specific markers (Figure 2B; Figure

438   S3). Mature neurons generated from wild type cells expressed markers of cortical

439   neurons and displayed electrophysiological characteristics typical of high quality iPSC-

440   derived neurons, including spontaneous action potentials and excitatory post-synaptic

441   currents (Figure 2D-F).

442

443   To assess the validity of iPSC-derived neurons to model *ACTL6B* mutation

444   syndrome, we sought to recapitulate the developmental expression increase[2] in *ACTL6B*

445   in wildtype neurons, where *ACTL6B* expression is absent from dividing cells but is

446   present in post-mitotic cells[2]. We found that *ACTL6B* increased in expression from day 1

447   to day 5. To minimize time in culture which can increase experimental variation, we

448   selected five days differentiation as our timepoint for post-mitotic transcriptomic analysis,

449   where we could be confident *ACTL6B* would be well expressed (Figure 3A and 3B). To

450   characterize the basic expression pattern of key genes involved in the BAF complex in

451   both p.*427Aspext*33 and control cells, we assessed the expression of *ACTL6B,*

452   *ACTL6A* and *SMARCA4* (MIM: 603254) a core DNA binding component of the BAF

453   complex. Genes were assessed at Day 0 (D0) and Day 5 (D5) of differentiation. *ACTL6B*

454   expression increased significantly in both p.*427Aspext*33 and control cells as cells

455   differentiated. We also detected a significant decrease of *ACTL6B* in p.*427Aspext*33

456   compared to control cells at D5 (Figure 3C). *ACTL6A* had high expression in proliferating

457   cells with a significant decrease after 5 days, but yet was still clearly expressed at day 5

458   in both control and p.*427Aspext*33 cells (Figure 3C). We detected no significant

459   difference in the expression level of *SMARCA4* between any cell line or timepoint (Figure

460   3C). To confirm and validate these mRNA based data, we performed western blot on

461   protein extracted from p.*427Aspext*33 and control cells at proliferative and post-mitotic

462   timepoints (Figure 3D). These data suggest that there is no difference in protein level of

463   any of BAF53A, BAF53B, and BRG1 between control and p.*427Aspext*33 cells. By

464   developmental period (proliferating and post-mitotic) we observe consistent protein

465   levels of BAF53A and BRG1, and absent BAF53B in proliferating cells.

466

467

468   **Engineered homozygous deletion of *ACTL6B* in human neurons causes severe**

469   **loss of dendrites**

470   What is the function of *ACTL6B* in developing human cells and what is its role in

471   human disease? Our previous experiments suggest that BAF53B is specific to post-

472   mitotic cells, as reported in rodents[22], so we opted to inactivate *ACTL6B* to determine

473   cellular phenotypes resulting from complete gene loss.

474   We knocked out *ACTL6B* from control human cells using a clonal genetic

475   engineering technique[23] (Supplemental Methods). We generated two independent

476   *ACTL6B* knockout cell lines that had different homozygous frameshift mutations in exon

477   1 (KO1 and KO2; referred to collectively as KO), and compared them to the isogenic cell

478   line that had undergone no editing event (Control) (Figure 4A-B). The use of two

479   independently edited cell lines with the same outcome (homozygous loss of *ACTL6B*) is

480   one way to ensure against cell line artefacts, where we do not expect the same artefact

481   to be present in both cell lines. To further ensure this, we Sanger Sequenced the five

482   genomic regions most likely to be edited by the gRNAs used, all of which were unedited,

483   suggesting no off-target effects, as has been reported and systematically assessed

484   previously[24]. We also performed long-range (1.6Kb) sequencing to ensure that these

485   mutations were in fact homozygous and not due to a large deletion in one allele, in

486   addition to DNA based qPCR to confirm equal gene dosage between edited and

487   unedited lines (Supplemental Methods). Following clonal gene editing and careful

488   genomic integrity assessment, we planned to investigate dendritic length anomalies in a

489   more mature neuronal state, since mouse KO *Actl6b* neurons show deficits in dendrite

490   development[4]. To do this, we differentiated human *ACTL6B* KO cell lines and their

491   matched isogenic controls for 15 days (D15 – a timepoint where we routinely see

492   extensive neuronal arborisation in culture[23]) and confirmed the loss of *ACTL6B*

493   expression at the mRNA and protein level (Figure 4C-D). We used MAP2 and TUJ1 as

494   dendritic and neuronal markers, respectively, since these are routinely used in

495   neuroscience research for this purpose [25; 26]. We observed virtually no MAP2 staining in

496   *ACTL6B* KO cells, while MAP2 was clearly present in most cells in the isogenic controls

497   (Figure 4E). We also observed a larger nuclear size in the deleted cells, as assayed by

498   DAPI, an effect that is obvious on cell examination (Figure 4F).

499   **The p.*427Aspext*33 mutation phenocopies *ACTL6B* KO dendritic deficits**

500   **and is reversible upon biallelic genetic repair**

501   From our genotype-phenotype data from affected individuals and their first

502   degree realtives, we reasoned that recessive mutations cause a loss-of-function of

503   *ACTL6B*, and thus may mimic the cellular phenotype of the engineered *ACTL6B* KO

504   cells. To demonstrate this, we reasoned that using these cell lines and comparing them

505   to a clonally repaired version should provide interpretable data.

506   We biallelicaly repaired the ACTL6Bext33 line to a wildtype genotype and

507   simultaneously reprogrammed these edited cell lines, where we had several

508   unsuccessful repairs that could be used as isogenic controls. Homology directed repair

509   was performed using a wildtype template in p.*427Aspext*33 fibroblasts plated at low

510   density and iPSCs colonies derived from a single fibroblast were isolated, ensuring

511   clonality and purity of repair[23]. After iPSC expansion of many colonies, we extracted

512   DNA and Sanger sequenced around the mutation site (Method S2-S4). A colony with

513   c.1279del mutation repaired to a wildtype genotype was identified and labelled as

514   Successful Repair (SR) and differentiated to NPCs in tandem with an Unsuccessful

515   Repair (UR) line, which was derived from a colony that received the CRISPR complex

516   and repair template but where no editing event occurred (Figure 5 A-B). We

517   differentiated these cells from NPCs to D15 neurons and then stained for MAP2 and

518   TUJ1, identical in design to the KO study. As shown in Figure 5D-E, affected individual

519   cells recapitulate the loss of MAP2 and increased nuclei size observed in the KO, a

520   result that is reversed on repair of the homozygous base change in *ACTL6B*.   The

521   similar cellular phenotype between affected individual and engineered KO neurons

522   suggest that the ACTL6Bext33 recessive mutation causes similar deficits to the

523   complete KO, and thus could be interpreted as causing a loss-of -function.

524

525   **Loss of dendrites due to loss of function of *ACTL6B* is likely due to delayed**

526   **maturation of young neurons**

527   Is the observed decrease in MAP2 staining due to immature differentiation,

528   differential differentiation, or a specific deficit in dendrite development? To try to address

529   these questions, we first asked whether the cell types in each condition were equivalent.

530   To investigate this question we stained D15 cultures from repaired and KO cells and

531   their control with an astrocyte (GFAP) and a neuronal marker (TUJ1), with the

532   hypothesis that perhaps deficits in *ACTL6B* bias NPCs towards becoming astrocytes.

533   Figure S4A shows the results of this experiment; we could not detect different numbers

534   of cells that stained for GFAP. We include in this experiment a positive control where we

535   add 0.1% BSA which can glialize cell cultures. To support the idea that deficits of

536   *ACTL6B* do not lead cell cultures to become more glial and to provide more specificity

537   than just GFAP, we assessed the transcriptomic data of p.*427Aspext*33 and control

538   cells we had generated in an RNA-Seq experiment. We found no consistent pattern in

539   mRNA expression levels of glial markers *ALDH1L1, GFAP*, and *GJA1* and neuronal

540   markers *RBFOX3* and *TUBB3* to suggest an increase in expression of glial related

541   genes in ACTL6Bext33 cells compared to control cells (Figure S4B)*.*   These data

542   indicate that deficits in *ACTL6B* do not lead NPCs to become more astrocytic. We

543 therefore ruled out the loss of MAP2 staining being due to cells being pushed towards an

544 astrocytic fate.

545 As a simple measurement of differentiation, we opted to photograph control,

546 ACTL6Bext.33, ACTL6B KO and Repair cells across several developmental timepoints.

547 Figure S5 shows that in contrast to repaired and control cell lines, unrepaired and KO

548 *ACTL6B* cells are not branched prior to day 20, whereas at day 25 through day 50, all

549 lines show branching.

550   These data suggest that deficits in *ACTL6B* lead to a delay in differentiation in

551 early post-mitotic states. This delay in differentiation, if true *in vivo*, may lead to cell

552 connectivity deficits.

553

554 **The p.*427Aspext*33 mutation alters BRG1 genomic binding and affects gene**

555 **expression**

556 This project began with the index case R3 (p.*427Aspext*33) which had fibroblasts

557 collected prior to mutation identification, thus our study is heavily biased towards this

558 case. To this end, we opted to continue experiments with these cells, with the idea that

559 we might recruit cells from other subjects or design exogenous templates for validation

560 studies.

561

562   We wanted to understand the molecular consequences of the p.*427Aspext*33

563 variant and how this might lead to neurodevelopmental deficits. Due to a lack of ChIP

564 grade antibodies directed specifically to BAF53B, we chose to perform a ChIP-Seq

565 experiment targeting BRG1, a key subunit of the BAF complex with ATPase activity that

566   is found both BAF53B and BAF53A containing BAF complexes [11]. We chose the D0 and

567   D5 time points for proliferating and post-mitotic cells respectively, and performed ChIP in

568   control and ACTL6Bext33 cells using eight replicates per subject per time period (32

569   ChIP experiments). We performed several QC experiments with different anti-BRG1

570   antibodies prior to sequencing to ensure appropriate parameters (not shown), and chose

571   two antibodies to provide overlapping datasets of Brg1-containing BAF complex binding

572   (Figure 6A). After sequencing and QC, we analyzed differential binding in D5 cells to

573   understand how the genomic targeting of Brg1-containing BAF complexes may be

574   altered by a mutant BAF53B subunit. ChIP peaks were called in at least 2/8 lines, and

575   differential analysis used reads from all replicates within the peak. 10,222 peaks were

576   common across all data points (Figure 6B), suggesting that BRG1 remains mostly at the

577   same location in the genome, even in mutant *ACTL6B* cells and irrespective of

578   developmental state.

579   We focused our primary analysis on D5, since this is when *ACTL6B* is

580   expressed, and tried to determine whether there was differential binding of BRG1 at

581   peaks called in both p.*427Aspext*33 and control cells. Using FDR <0.05, we found no

582   significant differences; however, using an uncorrected p-value of 0.05 revealed 382

583   common genomic regions that were significantly differentially bound and every one of

584   these showed increased binding in affected individual cells (Figure 6C). Loss-of-function

585   of BAF53B may lead to increased affinity or stabilization of the BAF complex to its

586   genomic targets, possibly through retention of BAF53A. More than half of the 382 sites

587   that BRG1-containing BAF complexes were found to bind to were associated with genes

588   (Figure 6C). PANTHER GO terms associated with the differentially bound regions were

589   related to cell adhesion and neurodevelopment (Figure 6D). This list included autism

590   associated genes including *AUTS2, PTEN, FOXP2*, and *SMARCA2*.

591   To further assess whether mutant *ACTL6B* leads to increased binding of BAF to

592   genomic regions, we performed a within-subjects analysis in proliferating (D0) and

593   differentiating (D5) cells, looking for peaks present at both developmental stages using

594   FDR<0.05 for peak calling. While we did not find the same peaks that were called

595   between cases and controls (suggesting the experiment was underpowered since we

596   used 8 replicates in each block), we found evidence for a general decrease in BRG1

597   binding in differentiated cells compared to proliferating cells in those genomic regions

598   present at both D0 and D5 in control conditions, in contrast to the p.*427Aspext*33 cells

599   where there was a consistent increase in BAF binding at D5 compared to D0 (Figure 6E)

600   at all sites. These data support the notion that a recessive *ACTL6B* mutation leads to

601   increased association of BRG1 to certain areas of the genome.

602

603   How does genomic BAF binding affect gene expression and how might this differ when

604   *ACTL6B* is mutated? We performed RNAseq in affected individual and control cells (n=4

605   independent replicates per subject) at D0 and D5 and looked only at those genes that

606   were detected in the ChIPSeq analysis. We were interested in those genes that showed

607   significant changes between D0 and D5 in the ChIPSeq data and which also showed

608   significant change in the RNAseq data between D0 and D5 (within-subjects); Also, we

609   selected those genes that showed RNAseq differences between mutant cells and control

610   cells at D5 (Table S2). We highlight *TPPP* (Table S4), a microtubule binding protein

611   involved in cell process extensions[27; 28], and *FSCN1*, which has been shown be involved

612   in neurite shape and trajectory in prior studies in mice[29]. Due to their biological function

613   and significance levels in our experiments, we chose to use *TPPP* and *FCSN1*

614   expression levels to assess the external validity of our findings. We note the prevalence

615   (Table S4) of genes that might be implicated in sphingolipid biology or myelin processing

616 (*SOX8*[30], *CERK*[31], and *A4GALT*[32]), consistent with Wu et al, (2007) who observed a

617 severe myelination defect in *Actl6b* KO mice.

618   We used *TPPP* and *FSCN1* expression as output markers to assess direct

619 versus correlational effects of mutant *ACTL6B*. We posed two initial questions to test

620 direct versus correlational effects. First; does the *ACTL6B* KO show a similar pattern of

621 expression to ACTL6Bext33 compared to its isogenic control? Second; do we see the

622 opposite effect in the UR cells compared to the SR cells?   We began by validating the

623 RNA-Seq data, using the same RNA that was used to make RNA-Seq libraries (Figure

624 7A). Next, we examined the expression of these genes between D0 and D5 timepoints in

625 *ACTL6B* KO cells and their isogenic controls, as well as in UR and SR cells. SR cells,

626 when compared to UR cells showed a significant increase in *TPPP* and decreased

627 expression of *FSCN1* as NPCs mature from D0 to D5. In *ACTL6B* knock-out cells

628 compared to their isogenic controls, we observed significant and opposite effects to that

629 observed with repaired cells: *FSCN1* expression did not decrease, while *TPPP*

630 expression did not increase as the cells differentiated (Figure 7A). These data provide

631 isogenic evidence that complete loss of *ACTL6B* and a repair of p.*427Aspext*33

632 recapitulate and reverse, respectfully, expression alterations in *TPPP* and *FSCN1* and

633 suggest that expression changes in these genes are directly caused by disruption of

634 *ACTL6B*.

635

636 **External validity of *TPPP* and *FSCN1* expression levels as markers of an *ACTL6B***

637 **recessive, loss-of-function disease in human neurons using constructs derived**

638 **from different *ACTL6B* variants.**

639   External validity can be provided by KO rescue and by recapitulating expression

640   effects using different mutations in *ACTL6B* identified in our cohorts (Figure 7B-D). If

641   *TPPP* and *FSCN1* expression levels are markers of loss-of-function of *ACTL6B*, the

642   exogenous re-introduction of *ACTL6B* on a KO background should help restore their

643   expression towards levels observed in lines with wild-type *ACTL6B*. Further, expressing

644   mutant *ACTL6B* to match other variants found in the recessive cohort should re-establish

645   expression changes on an *ACTL6B* KO background. We therefore made *ACTL6B*

646   constructs of two recessive mutations c.441_443 del and c.1275C>A, and the most

647   prevalent dominant mutation c.1027 G>A, as well as the WT construct itself. Expressing

648   these variants from trasnsiently delivered vector on an *ACTL6B* KO background, may

649   give us an indication if the dominant and recessive variants mediate their effects through

650   the same molecular pathways and cause similar effects on the expression of *FSCN1* and

651   *TPPP*. At a D5 timepoint, cells transfected with WT *ACTL6B* showed decreased

652   expression of *FSCN1* and increased expression of *TPPP*, consistent with what we

653   observed in the initial KO experiment (Figure 7D), meaning that the WT construct can

654   rescue the expression changes observed in *ACTL6B* KO cells. We observed that the

655   two recessive variants (c.441_443 del and c.1275C>A) mimicked the effects observed in

656   the recessive p.*427Aspext*33 variant, while the dominant mutation mimicked wildtype

657   cells (Figure 7D).

658

659   **Confirmation of dendritic deficits and gene expression markers using neurons**

660   **derived from *ACTL6B* mutant c.617T>C/ c.724C>T**

661   We obtained fibroblasts from individual R9 with compound heterozygous

662   mutations in *ACTL6B* (c.617T>C, p.Leu206Pro and c.724C>T, p.Gln242*) (Table 1). We

663   induced the fibroblasts to become iPSCs, differentiated the iPSCs to D15 neurons and

664   confirmed the mutant genotype of this line (Figure 8A-B). We compared this "*ACTL6B*

665   compound heterozygous mutant" line to healthy control cells differentiated to a day 15

666   timepoint, and found a similar decrease of *MAP2* staining and increased nuclei size as

667   compared to the *ACTL6B* KO and ACTL6Bext33 lines (Figure 8C-D). Assessing the

668   expression of *TPPP* and *FSCN1* at D5 and D0 timepoints in the *ACTL6B* compound

669   mutant and control lines also produced results similar to those seen with the

670   ACTL6Bext33 line, with the *ACTL6B* compound mutant showing a lack of increased

671   expression of *TPPP*, as well as a lack of decreased expression of *FSCN1* during

672   differentiation compared to control cells (Figure 8E).

673

Discussion

674

675   These data describe two distinct neurodevelopmental diseases caused by

676 dominant or recessive mutations in *ACTL6B*. This work positions *ACTL6B* mutations as

677 causing both a recessive neurological disease characterized by severe epileptic

678 encephalopathy, and a dominant intellectual disability syndrome with severe speech and

679 ambulation deficits.

680   Previous studies have identified mutations in genes that code for other subunits

681 of the nBAF and npBAF complexes that are capable of causing disease through

682 dysregulated BAF function, collectively called "Bafopathies"[33]. The two foremost

683 diseases among the Bafopathies, Coffin-Siris (CSS) (MIM: 135900) and Nicolaides–

684 Baraitser (NCBRS) (MIM: 601358) syndrome show interesting parallels and differences

685 to the diseases described here[34; 35]. While NCBRS is a monogenic disease, caused

686 exclusively by mutations in *SMARCA2* (MIM: 600014) that are autosomal dominant, and

687 CSS is a genetically diverse disease, and can be caused by mutations in *ARID1B* (MIM:

688 614556) and a variety of other genes that play a role in the BAF complex, that vary in

689 their inheritance pattern, common symptoms appear to exist in both these conditions and

690 the diseases described here. Common symptoms reported across conditions include

691 intellectual disability, developmental delay, hypotonia and some form of dysmorphic

692 facial features [34]. Like individuals with recessive mutations in *ACTL6B*, individuals with

693 NCBRS also show early-onset seizures[36], and seizures are also reported in individuals

694 with CSS, although they are not necessarily early-onset [34; 37; 38]. Individuals with NCBRS

695 also show short phalanges[36], as observed in some individuals with dominant mutations

696 in *ACTL6B*. However, some of the specific developmental symptoms observed in these

697 diseases, such as sparse scalp hair[39] or an absent fifth digit[36] do not appear in

698 individuals with either recessive or dominant mutations in *ACTL6B*. This could suggest

699   that while a general disruption of the BAF complex in a variety of protein subunits

700   neurodevelopment will inevitably lead to intellectual disability and developmental delay,

701   the specific protein subunit that is affected will determine the presence and nature of

702   dysmorphisms and epilepsy.

703   To understand why mutations in *ACTL6B* cause disease, we modeled the

704   disease in human NPCs and neurons. We first confirmed that *ACTL6B* expression was

705   induced upon neural cells becoming post-mitotic. We then went on to make several

706   different cell models in the hope of reducing variation across experimental variables. We

707   made forebrain progenitor cells from a healthy individual with experimentally induced

708   knock-out of *ACTL6B* to understand the effects of complete loss of the gene, in addition

709   to cells derived from individuals R9 and R3 with an isogenic engineered repaired cell

710   line.

711   While we cannot precisely determine the mechanism of the disease that appears

712   to be caused by bi-allelic mutations in *ACTL6B*, our results do illuminate several key

713   features of the etiology of the disease. First, the presence of BAF53B in the

714   ACTL6Bext33 cell line at D5 eliminates the possibility that the symptoms are caused by

715   an absence of BAF53B, as is likely the case in other variants of BAF53B where NMD is

716   predicted to occur[19]. Instead, it seems plausible that the symptoms are the result of a

717   loss of function of BAF53B stemming from changes in the structure of the protein. This

718   hypothesis is supported by our observations in the *ACTL6B* KO model, which shows

719   similar deficits in both MAP2 staining and the expression of key genes identified in the

720   ACTL6Bext33 that are regulated by BAF. *ACTL6B* KO cells expressing the recessive

721   mutations in *ACTL6B* observed in our recessive cohort fails to rescue aberrant

722   expression of genes, whereas reintroduction of wildtype *ACTL6B* does, strongly

723   suggesting that the phenotype is the result of a loss of function.

724   However, how the recessive mutations render BAF53B non-functional could be

725   due to one of several possibilities. Perhaps the most intuitive answer is that mutations

726   disrupt the ability of BAF53B to bind to the BAF complex. If this fails to occur, this might

727   allow BAF53A to remain bound in the complex. Given that there are a great many BAF

728   complexes that dynamically exchange parts to affect cell differentiation at any one time,

729   a high proportion of BAF53A in BAF might cause increased affinity of BAF to the

730   genome in a differentiating cell state compared to both a proliferating cell state when

731   BAF53B is absent or a differentiated cell state where BAF53B is present but not

732   functional and/or when the interaction with the complex is impaired. The increased

733   presence of BAF53A in the BAF complex, associated with a more proliferative neuronal

734   cell state, might also explain the delayed differentiation we observed in disease cells.

735   Another explanation could be that recessive mutations do not prevent BAF53B from

736   binding to the BAF complex, but instead prevent the various components of the complex

737   from interacting properly, and thus prevent the BAF complex from interacting with the

738   genome and other proteins in yet unknown ways. Finally, there is the possibility that

739   recessive mutations do not disrupt BAF complex function significantly at all, but instead

740   prevent BAF53B from properly interacting with the other complexes such as SRCAP[40],

741   TIP60/NuA4[19] and INO80[41]. Future work will need to look at how mutant BAF interacts

742   with different proteins.

743

744   With respect to the dominant mutation identified in eight unrelated individuals, we failed

745   to observe the transcription effects we found in the KO, *ACTL6B* compound

746   heterozygous mutant or the ACTL6Bext33 cells, suggesting dominant and recessive

747   mutations in *ACTL6B* cause disease through distinct molecular pathways. This is also

748   consistent with the observation of different symptoms in individuals with recessive/

749   dominant mutations in *ACTL6B*. Based on the limited molecular information we have for

750   dominant mutations, there exists many potential explanations for how a point mutation in

751   *ACTL6B* might cause the observed symptoms. Given that these subjects all have a

752   functioning copy of BAF53B which presumably incorporates normally into BAF or other

753   complexes, it is reasonable to suggest that the *ACTL6B* dominant mutations identified

754   here may be gain-of-function. One of the few clues that we have at this stage of

755   investigation is that the highly specific nature of the p.Gly343Arg variant suggests a very

756   precise interaction is being disrupted or created. Previous work in mice[42] has shown that

757   deletion of the hydrophobic domain of BAF53b results in a dominant negative form of

758   the protein, causing deficits in memory, LTP, and gene expression. These deficits were

759   likely caused by altering the ability BAF53B to interact with other proteins[42]. It is possible

760   that the dominant mutations observed in this study cause disease by altering the

761   hydrophobic domain of BAF53B through a similar mechanism.

762

763   Several genes of note may be important targets of the BAF complex at different

764   developmental stages. *FSCN1* is one of these and is strongly associated with the

765   formation of actin, particularly in early neurodevelopment[29; 43]. The lack of increase of

766   *FSCN1* observed in our models of *ACTL6B* dysfunction as cells differentiate may

767   therefore be the result of neuronal cells remaining in a more proliferative or immature

768   state due to an impairment in the ability of *ACTL6B* to transition the BAF complex from

769   promoting genes associated with proliferation to those associated with neuronal

770   outgrowth[44].

771   The stable expression levels of *TPPP* observed in models of *ACTL6B*

772   dysfunction as NPCs differentiate may reflect the cytoskeletal changes observed both

773   within our own models and in the deficits in dendritic spine and synapse function

774 observed in mouse models of *Actl6b* KO. It should also be noted that our ChIP-SEQ

775 data that initially highlighted these genes as being dysregulated is based upon only

776 BRG1-containing BAF complexes. As BRG1 and BRM are mutually exclusive

777 components of the BAF complex that are both found in dividing and post-mitotic neural

778 cells[11], it is possible that the dataset we generated is only a partial picture of the regions

779 of the genome where BAF may bind in these cells.

780 This work brings together extensive clinical samples and human stem cell

781 modeling to demonstrate that mutations in *ACTL6B* in human cause severe neurological

782 disorders. Substantially more work will need to be done to understand the precise

783 mechanisms of how recessive or dominant mutations in *ACTL6B* affect incorporation into

784 the BAF complex, and how this incorporation can alter differential genomic binding and

785 gene expression patterns.

786

787 **Supplemental Data**

788 Supplemental Data can be found with this article online and includes five supplementary

789 figures, four supplementary tables and supplementary methods which provide additional

790 clinical details of individuals and further details of the generation, characterization, and

791 quality control of the cell lines generated in this study.

804

805

Figure Legends

807 **Figure 1. Location of mutations in *ACTL6B* found in individuals with potential**
808 **recessive or dominant disease causing mutations**

809 A) Photos of individuals with *ACTL6B* mutations**.** Note broad mouth of individuals D1,
810 D2, D3 and D7, diastema in D1, D3, D7, bulbous tip of the nose in all D individuals, and
811 hypertelorism with telecanthi in individual D8. Lower right: MRI images of individuals with
812 recessive *ACTL6B* mutations. For individual R4, note white matter T2 hyperintensity
813 (arrows). For individual R8, note enlarged lateral ventricles and asymmetric gyral pattern
814 (left, arrows). On the right, note thin corpus callosum (arrows). B) Linear graph of
815 mutations in *ACTL6B* (introns not drawn to scale). C) Conservation of the residues
816 affected by amino acid substitutions. D) 3D model generated with SWISSMODEL based
817 on S. cerevisiae Arp4 (yeast homolog of ACTL6B), visualized with Swiss-PdbViewer
818 showing that recessive mutations are not focused in one region. Note however that the
819 dominant mutations seem to lie at the periphery of the protein thus they might affect
820 protein-protein interactions.

821

822 **Figure 2. Generation of iPSC-derived neurons for BAF53 studies**

823 A) Representative images of quality control staining done on iPSCs. B) Representative
824 quality control staining on NPC cultures. C) Representative staining of control cells for
825 TUJ1 and MAP2 at D15 of differentiation. D) Representative trace of miniature EPSCs
826 from D25 neurons held at -40 mv. E) Representative recordings showing spontaneous
827 activity of D25 neurons in current-clamp mode. F) Trace of a hyperpolarizing pulse
828 showing a depolarizing sag followed by multiple rebound action potentials. The first
829 action potential is shown at a higher temporal resolution. All scale bars represent 40 µm

830

831 **Figure 3. Comparison of control and ACTL6Bext*33 before and after expression of**
832 ***ACTL6B***

833 A) Diagram illustrating the production of control and ACTL6Bext*33 iPSC-derived NPCs
834 from fibroblasts B) *ACTL6B* expression normalized to *GAPDH* expression plotted against
835 number of days of differentiation of NPCs. N=4, error bars represent standard error
836 around the mean. C) Expression of key genes in the SWI/SWF complex in 706
837 ACTL6Bext*33 and control NPCs in proliferating and post-mitotic states. Genes are
838 normalized to GAPDH expression. (n≥3) Student's t-test, *P<0.05, **P<0.01. H) Western
839 blots assessing the level of proteins encoded by the genes displayed in G.

840

841 **Figure 4. Generation and characterization of *ACTL6B* KO neurons reveals a loss of**
842 **dendrites.**

843 A) Diagram of the experimental approach taken to generate *ACTL6B* KO NPCs. B)
844 Sanger sequencing traces of two *ACTL6B* KO lines. C) *ACTL6B* expression in control
845 and *ACTL6B* KO NPCs at a D0 and D5 timepoint (n≥3) D) Western Blots assessing the

846　protein levels of *BAF53A/B* in ACTL6B KO lines. E) Representative TUJ1 and MAP2
847　staining of control and *ACTL6B* KO D15 immature forebrain neurons. F) Quantification of
848　the surface area of the nucleus in the cell lines shown in E, (n>50). Student's t-test,
849　*P<0.05, **P<0.01.

850

851　**Figure 5. Repair of the *ACTL6B* c.1279del mutation restores morphological and**
852　**dendritic deficits.**

853　A) Schematic detailing *ACTL6B* CRISPR repair. B) Sanger sequencing traces of a
854　Successful Repair (SR) and Unrepaired (UR) cell line generated from ACTL6Bext*33 cell
855　line. C) *ACTL6B* expression in SR and UR NPCs at a D5 timepoint (n=6) D)
856　Representative TUJ1 and MAP2 staining taken from SR and UR forebrain immature
857　neurons at D15. Scale bars represent 40μm. E) Quantification of the surface area of the
858　nucleus and soma, and the length of projections in the cell lines shown in D, (n>50).
859　Student's t-test *P<0.05, **P<0.01, ***P<0.001

860　**Figure 6. ACTL6Bext*33 variant leads to increased binding of BRG1-BAF complex**
861　**to the genome.**

862　A) Diagram illustrating the ChiP-Seq experiment. B) Venn diagram showing overlap of
863　genes that the BRG1 complex is bound to. C) Decreased binding at all 382 FDR
864　significant sites in control cells compared to ACTL6Bext*33 cells (pink dots are
865　significant, while blue dots are not). D) Proportion of BRG1 binding sites found in relation
866　to their proximity to a gene. E) Gene ontology analysis of differentially bound regions. F)
867　Within-subjects differential binding across developmental stages (D0 and D5) showing
868　decreased binding in D0 compared to D5 in ACTL6Bext*33 cells (pink dots are
869　significant, while blue dots are not). Genes showing a significant difference (FDR-
870　adjusted p-values (Benjamini-Hochberg) ≤0.05) in D5 relative to D0 using a GLM as
871　implemented in DESeq2.

872

873　**Figure 7. External validity in multiple *ACTL6B* mutant models in human neurons**

874　A) *TPPP* and *FSCN1* expression in initial RNA-Seq (n≥4) and qPCR (n≥3) data
875　(ACTL6Bext*33 vs control); unrepaired (UR) ACTL6Bext*33 vs ACTL6Bext*33
876　Successful Repair (SR) (n=6); and *ACTL6B* KO vs isogenic control cells (n=5). Results
877　are represented as mean ± SEM. Student's t-test *P<0.05, **P<0.01, ***P<0.001 B)
878　Experimental plan for generation of multiple human neuronal cell lines expressing
879　various mutant *ACTL6B* constructs. C) Brightfield and GFP images demonstrating high
880　transfection of *ACTL6B* constructs. D) mRNA expression in transfected *ACTL6B* KO
881　NPCs at D5 timepoints of *ACLT6B*, *TPPP,* and *FSCN1* (E) (n=3). Results are
882　represented as mean ± SEM. Student's t-test *P<0.05, **P<0.01, ***P<0.001

883

884　**Figure 8. Neurons derived from an individual with a compound mutation in**
885　***ACTL6B* show a similar phenotype to ACTL6Bext33 and ACTL6B KO neurons.**

886 A) Schematic showing generation of ACTL6Bcompoundmutant NPCs B) Sanger
887 sequencing traces of ACTL6Bcompoundmutant and control cell line at both identified
888 point mutations in the *ACTL6B* gene C) Representative TUJ1 and MAP2 staining of
889 control and ACTL6Bcompoundmutation immature forebrain neurons. D) Quantification of
890 the surface area of the nucleus in the cell lines shown in E. E) *TPPP* and *FSCN1*
891 expression in ACTL6Bcompoundmutant vs control cells at mitotic (D0) and post-mitotic
892 (D5) timepoints (n>50). Student's t-test, *P<0.05, **P<0.01.

893

894

895

896

897

Table 1. Pathogenic variants and key clinical information of individuals with bi-allelic
mutations in *ACTL6B*.

Individual	R1	R2		R3	R4		R5		R6		R7	R8a	R8b	R9		R10
Inheritance	Recessive, homozygous	Recessive, Compound heterozygous. Similarly affected brother passed away at 5y		Recessive, homozygous. Similarly affected brother passed away at 4y	Recessive, Compound heterozygous		Recessive, Compound heterozygous		Recessive, Compound heterozygous		Recessive, homozygous	Recessive, homozygous.	Recessive, homozygous. Sister of R8a.	Recessive, Compound heterozygous		Recessive, homozygous
Coding Change (NM_016188.4)	c.441_443delCTT	c.695delC	c.1275C>A	c.1279del	c.389G>A	c.556C>T	c.852C>G	c.740G>A	c.1231C>T	c.669+1G>A	c.289C>T	c.1045G>A	c.1045G>A	c.724C>T	c.617T>C	c.1279del
Protein Change (NP_057272.1)	p.Phe147del	p.Pro232Glnfs*24	p.Cys425*	p.*427Aspext*33	p.Arg130Gln	p.Gln186*	p.Tyr284*	p.Trp247*	p.Gln411*	splicing	p.Arg97*	p.Gly349Ser	p.Gly349Ser	p.Gln242*	p.Leu206Pro	p.*427Aspext*33
gnomAD MAF	0.000001444, no homozygotes	Absent	Absent	Absent	0.00000 8132, no homozyg	Absent	Absent	Absent	Absent	Absent	0.00000 4064, no homozyg	0.00000 12119, no homo	0.00000 12119, no homo	Absent	Absent	Absent

	3y F	5y M (passed away at age 5)	11m M (passed away age 5)	ote s 8y F	5m F	12m M (passed away age 2)	ote s 4y F	zyg ote s 6y F	zyg ote s 5y F	14m F	4.5y F
Age at assessment	3y F	5y M (passed away at age 5)	11m M (passed away age 5)	8y F	5m F	12m M (passed away age 2)	4y F	6y F	5y F	14m F	4.5y F
Head circum. In cm	43 (-3.5 SD)	NA	44 (3rd)	50.3 (10th %ile)	38,4 (-3.0 SD)	42 (-2.4 SD)	Nl	18 m 41.5 (-3.8 SD)	4m 39 (7th %ile)	43 (-2,5 SD)	47 (-2.8 SD)
ID, DD	+, Severe	+	+	+, Severe	+, Severe	+, Severe	+, Severe	+, Severe	+, Severe	+, Severe	+
Speech	-	-	NA	-	NA	-	NA	-	-	-	-
Ambulation	-	-	NA	-	NA	-	NA	-	-	-	+, with support
Axial hypotonia	+	+	+	+	+	+	+	+	+	+	+
Limb spasticity	+	+	+	+	+	+	+	+	+	+	+
Feeding difficulties	+	+	+	-	+	+	+	+	+	+	-
Epilepsy	+	+	+	+	+	+	+	+	+	+	+
Seizures (age at beginning)	3 months	3y	NA	NA	2 months	Neonatal (25 days)	Infancy	Infancy	Infancy	Antenatal	9 months, infantile

											spasms
Seizure types	Myoclonias 2-6 per day	Complex partial	NA	NA	Tonic and myoclonic	Focal onset epilepsy, progressed to infantile spasms	NA	NA	NA	myoclonic seizures AND tonic seizures	Tonic and myoclonic
EEG anomalies	Multifocal epileptic activity	NA	Multifocal epileptic activity	NA	Multifocal epileptic activity	Multifocal interictal epileptiform spike discharges, lack of posterior dominant rhythm	Multifocal EEG abnormalities	generalized slowing of background rhythms	generalized slowing of background rhythms	Multifocal epileptic activity, esp. left hemisphere	Multifocal epileptic activity, esp. left hemisphere
MRI	Prominent subarachnoid spaces and small corpus callosum	Normal	Mild T2 hyperintensity in frontal periventricular white matter	Mild T2 hyperintensity in frontal periventricular white matter	2 months of age showed symmetric signal changes in the brainstem and in the dorsal medulla oblongata, possibly also around	3 w.o.: asymmetric ventricles, cortical dysplasia right parietal lobe. 9 m: cerebral atrophy, hypoplasia of corpus callosum	NA	MRI at 5mo: Significantly decreased white matter throughout, extr	10 mo: Periventricular leukomalacia with white matter volume loss,	Thin corpus callosum High signal intensity doral globus pallidus/putamen Some asymmetry gyral patern	At 3.5yo: Cerebral and cerebellar atrophy, thin corpus callosum

				the dentate nucleus			emely thin corpus callosum. Normal MR spectroscopy	overall brain volume loss, delayed myelination and thinning of corpus callosum. Normal MR spectroscopy		

900

901

902

903

904

905

909   Table 2. Pathogenic variants and key clinical information of individuals with *de novo*

910   mutations in *ACTL6B*.

Individual	D1	D2	D3	D4	D5	D6	D7	D8	D9	D10
Coding Change (NM_016188.4)	c.1027G>A	c.1027G>A	c.1027G>A	c.1027G>A	c.1027G>A	c.1027G>A	c.1027G>A	c.1027G>A	c.230A>G	c.1027G>C
Protein Change (NP_057272.1)	p.Gly343Arg	p.Gly343Arg	p.Gly343Arg	p.Gly343Arg	p.Gly343Arg	p.Gly343Arg	p.Gly343Arg	p.Gly343Arg	p.Asp77Gly	p.Gly343Arg
gnomAD MAF	Absent	Absent	Absent	Absent	Absent	Absent	Absent	Absent	Absent	Absent
Age at assessment	5y6m M	29y F	6y6m M	5y9m F	4y6m F	3y F	21y F	2y 6m F	8y F	12yF
Head circum. In cm	49 (-2.1 SD)	53 cm (11th %ile)	51 cm at age 5 yr (50th centile)	48.6 (-2.2 SD)	48 cm (2nd %ile)	48.0 cm (20th %ile)	52.2 cm (-2.0 SD)	45.5 cm (-0.1 SD)	50th-75th %ile	52 (-1,-2SD)
Degree of	Seve	Seve	Seve	Seve	Seve	Seve	Sever	Sever	Seve	Seve

ID/DD	re	re	re	re	re	re	e	e	re	re
Speech	-	-	-	10-20 words, Receptive skills better	-	-. Gestures.	-	-	-. Gestures. Receptive skills better	One word
Ambulation	-	+	limited	Delayed. Wide based gait	-	-	-	-	NA	Delayed. Wide based gait
Hypotonia	NA	+	+	NA	+	+	NA	-	NA	+
Autism spectrum disorder	NA	+	Unknown	+	NA	NA	NA	-	+	-
Features of ASD	NA	NA	+	NA	stereotypies	NA	hand wringing	-	NA	stereotypies
Seizure disorder	-	-	-	-	-	-	Infantile spasms and GTCS	-	NA	-
MRI	NA	NA	NA	NA	NA	thinning of the corpus callosum	Generalised atrophy at 2y	mild periventricular gliosis	NA	Nl

Wide or prominent forehead	+	+	+	+	-	-	+	+	+	-
Hypertelorism	+	+	+	-	-	+	-	+	+	-
Wide mouth	+	+	+	-	-	-	+	+	NA	+
Short phalanges or nails	NA	+	-	+	-	-	+	-	+	-

911

Web Resources

913   BWA: http://bio-bwa.sourceforge.net/

914   GATK: https://software.broadinstitute.org/gatk/

915   MACS2: https://github.com/taoliu/MACS/wiki/Install-macs2

916   Trim Galore: http://www.bioinformatics.babraham.ac.uk/projects/trim_galore/

917   Bioconductor: http://bioconductor.org/packages/release/bioc/html/DiffBind.html

918   HOMER: http://homer.ucsd.edu/homer/

919   Neurolucida: https://www.mbfbioscience.com/neurolucida

920   Imagelab: http://www.bio-rad.com/en-ca/product/image-lab-software6\

921   Online Mendelian Inheritance in Man: http://www.omim.org

922   VarSome: https://varsome.com/

923

924

925   **<u>References</u>**

926   1. Meagher, R.B., Kandasamy, M.K., Deal, R.B., and McKinney, E.C. (2007). Actin-related
927   proteins in chromatin-level control of the cell cycle and developmental transitions.
928   Trends in cell biology 17, 325-332.
929   2. Biggar, S.R., and Crabtree, G.R. (1999). Continuous and widespread roles for the Swi-Snf
930   complex in transcription. EMBO J 18, 2254-2264.
931   3. Lessard, J., Wu, J.I., Ranish, J.A., Wan, M., Winslow, M.M., Staahl, B.T., Wu, H., Aebersold, R.,
932   Graef, I.A., and Crabtree, G.R. (2007). An essential switch in subunit composition of a
933   chromatin remodeling complex during neural development. Neuron 55, 201-215.
934   4. Wu, J.I., Lessard, J., Olave, I.A., Qiu, Z., Ghosh, A., Graef, I.A., and Crabtree, G.R. (2007).
935   Regulation of dendritic development by neuron-specific chromatin remodeling
936   complexes. Neuron 56, 94-108.
937   5. Peterson, C.L. (1996). Multiple SWItches to turn on chromatin? Curr Opin Genet Dev 6,
938   171-175.
939   6. Sudarsanam, P., and Winston, F. (2000). The Swi/Snf family nucleosome-remodeling
940   complexes and transcriptional control. Trends Genet 16, 345-351.
941   7. Yoo, A.S., Staahl, B.T., Chen, L., and Crabtree, G.R. (2009). MicroRNA-mediated switching of
942   chromatin-remodelling complexes in neural development. Nature 460, 642-646.
943   8. Staahl, B.T., and Crabtree, G.R. (2013). Creating a neural specific chromatin landscape by
944   npBAF and nBAF complexes. Curr Opin Neurobiol 23, 903-913.
945   9. Vogel-Ciernia, A., Matheos, D.P., Barrett, R.M., Kramar, E.A., Azzawi, S., Chen, Y., Magnan,
946   C.N., Zeller, M., Sylvain, A., Haettig, J., et al. (2013). The neuron-specific chromatin
947   regulatory subunit BAF53b is necessary for synaptic plasticity and memory. Nature
948   neuroscience 16, 552-561.
949   10. Santen, G.W.E., Kriek, M., and van Attikum, H. (2012). SWI/SNF complex in disorder:
950   SWItching from malignancies to intellectual disability. Epigenetics 7, 1219-1224.
951   11. Sokpor, G., Xie, Y., Rosenbusch, J., and Tuoc, T. (2017). Chromatin Remodeling BAF
952   (SWI/SNF) Complexes in Neural Development and Disorders. Frontiers in molecular
953   neuroscience 10, 243-243.
954   12. Bakshi, R., Hassan, M.Q., Pratap, J., Lian, J.B., Montecino, M.A., van Wijnen, A.J., Stein, J.L.,
955   Imbalzano, A.N., and Stein, G.S. (2010). The human SWI/SNF complex associates
956   with RUNX1 to control transcription of hematopoietic target genes. J Cell Physiol
957   225, 569-576.
958   13. Bell, S., Hettige, N., Silveira, H., Peng, H., Wu, H., Jefri, M., Antonyan, L., Zhang, Y., Zhang,
959   X., and Ernst, C. (In Press). Differentiation of Human Induced Pluripotent Stem Cells
960   (iPSCs) into an Effective Model of Forebrain Neural Progenitor Cells and Mature
961   Neurons. Bio-protocol.
962   14. Bell, S., Peng, H., Crapper, L., Kolobova, I., Maussion, G., Vasuta, C., Yerko, V., Wong, T.P.,
963   and Ernst, C. (2017). A Rapid Pipeline to Model Rare Neurodevelopmental Disorders
964   with Simultaneous CRISPR/Cas9 Gene Editing. Stem Cells Transl Med 6, 886-896.
965   15. Reynolds, B.A., and Weiss, S. (1996). Clonal and population analyses demonstrate that an
966   EGF-responsive mammalian embryonic CNS precursor is a stem cell. Dev Biol 175,
967   1-13.
968   16. Langmead, B., Trapnell, C., Pop, M., and Salzberg, S.L. (2009). Ultrafast and memory-
969   efficient alignment of short DNA sequences to the human genome. Genome Biol 10,
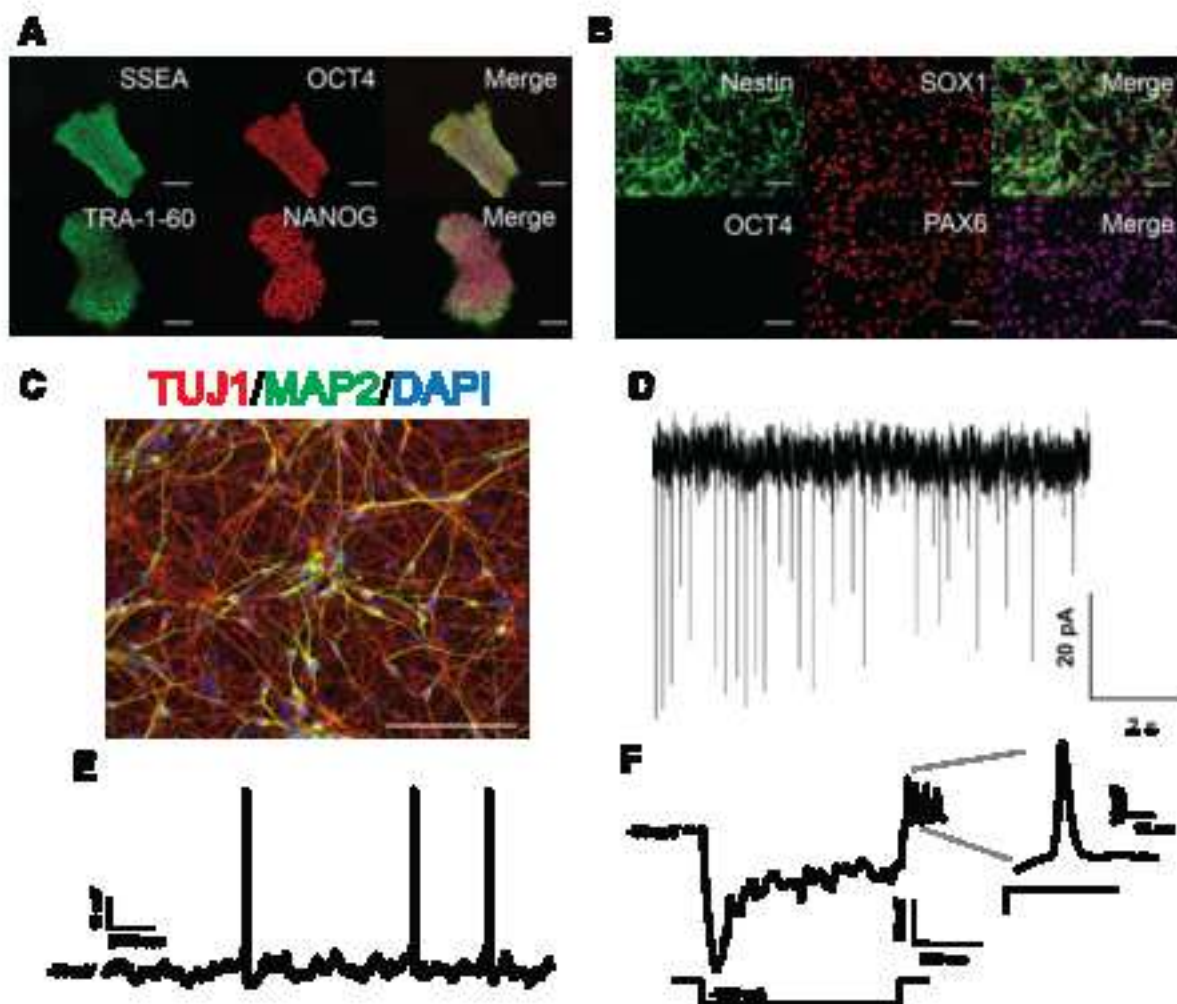970   R25.

971   17. Trapnell, C., Roberts, A., Goff, L., Pertea, G., Kim, D., Kelley, D.R., Pimentel, H., Salzberg,
972   S.L., Rinn, J.L., and Pachter, L. (2012). Differential gene and transcript expression
973   analysis of RNA-seq experiments with TopHat and Cufflinks. Nat Protoc 7, 562-578.
974   18. Chen, E.S., Gigek, C.O., Rosenfeld, J.A., Diallo, A.B., Maussion, G., Chen, G.G., Vaillancourt,
975   K., Lopez, J.P., Crapper, L., Poujol, R., et al. (2014). Molecular convergence of
976   neurodevelopmental disorders. Am J Hum Genet 95, 490-508.
977   19. Khajavi, M., Inoue, K., and Lupski, J.R. (2006). Nonsense-mediated mRNA decay
978   modulates clinical outcome of genetic disease. European journal of human genetics :
979   EJHG 14, 1074-1081.
980   20. Dominguez, R., and Holmes, K.C. (2011). Actin structure and function. Annual review of
981   biophysics 40, 169-186.
982   21. Holmes, K.C., Popp, D., Gebhard, W., and Kabsch, W. (1990). Atomic model of the actin
983   filament. Nature 347, 44-49.
984   22. Yoo, M., Choi, K.Y., Kim, J., Kim, M., Shim, J., Choi, J.H., Cho, H.Y., Oh, J.P., Kim, H.S., Kaang,
985   B.K., et al. (2017). BAF53b, a Neuron-Specific Nucleosome Remodeling Factor, Is
986   Induced after Learning and Facilitates Long-Term Memory Consolidation. J Neurosci
987   37, 3686-3697.
988   23. Bell, S., Maussion, G., Jefri, M., Peng, H., Theroux, J.F., Silveira, H., Soubannier, V., Wu, H.,
989   Hu, P., Galat, E., et al. (2018). Disruption of GRIN2B Impairs Differentiation in
990   Human Neurons. Stem Cell Reports 11, 183-196.
991   24. Veres, A., Gosis, B.S., Ding, Q., Collins, R., Ragavendran, A., Brand, H., Erdin, S., Cowan,
992   C.A., Talkowski, M.E., and Musunuru, K. (2014). Low incidence of off-target
993   mutations in individual CRISPR-Cas9 and TALEN targeted human stem cell clones
994   detected by whole-genome sequencing. Cell stem cell 15, 27-30.
995   25. Harada, A., Teng, J., Takei, Y., Oguchi, K., and Hirokawa, N. (2002). MAP2 is required for
996   dendrite elongation, PKA anchoring in dendrites, and proper PKA signal
997   transduction. The Journal of cell biology 158, 541-549.
998   26. Goedert, M., Crowther, R.A., and Garner, C.C. (1991). Molecular characterization of
999   microtubule-associated proteins tau and MAP2. Trends Neurosci 14, 193-199.
1000   27. Skjoerringe, T., Lundvig, D.M., Jensen, P.H., and Moos, T. (2006). P25alpha/Tubulin
1001   polymerization promoting protein expression by myelinating oligodendrocytes of
1002   the developing rat brain. J Neurochem 99, 333-342.
1003   28. Mino, R.E., Rogers, S.L., Risinger, A.L., Rohena, C., Banerjee, S., and Bhat, M.A. (2016).
1004   Drosophila Ringmaker regulates microtubule stabilization and axonal extension
1005   during embryonic development. Journal of Cell Science 129, 3282-3294.
1006   29. Kraft, R., Escobar, M.M., Narro, M.L., Kurtis, J.L., Efrat, A., Barnard, K., and Restifo, L.L.
1007   (2006). Phenotypes of Drosophila brain neurons in primary culture reveal a role for
1008   fascin in neurite shape and trajectory. J Neurosci 26, 8734-8747.
1009   30. Stolt, C.C., Lommes, P., Friedrich, R.P., and Wegner, M. (2004). Transcription factors Sox8
1010   and Sox10 perform non-equivalent roles during oligodendrocyte development
1011   despite functional redundancy. Development (Cambridge, England) 131, 2349-2358.
1012   31. Boggs, J.M., Gao, W., Zhao, J., Park, H.J., Liu, Y., and Basu, A. (2010). Participation of
1013   galactosylceramide and sulfatide in glycosynapses between oligodendrocyte or
1014   myelin membranes. FEBS Lett 584, 1771-1778.
1015   32. Kaczmarek, R., Mikolajewicz, K., Szymczak, K., Duk, M., Majorczyk, E., Krop-Watorek, A.,
1016   Buczkowska, A., and Czerwinski, M. (2016). Evaluation of an amino acid residue
1017   critical for the specificity and activity of human Gb3/CD77 synthase. Glycoconjugate
1018   Journal 33, 963-973.
1019   33. Aref-Eshghi, E., Bend, E.G., Hood, R.L., Schenkel, L.C., Carere, D.A., Chakrabarti, R.,
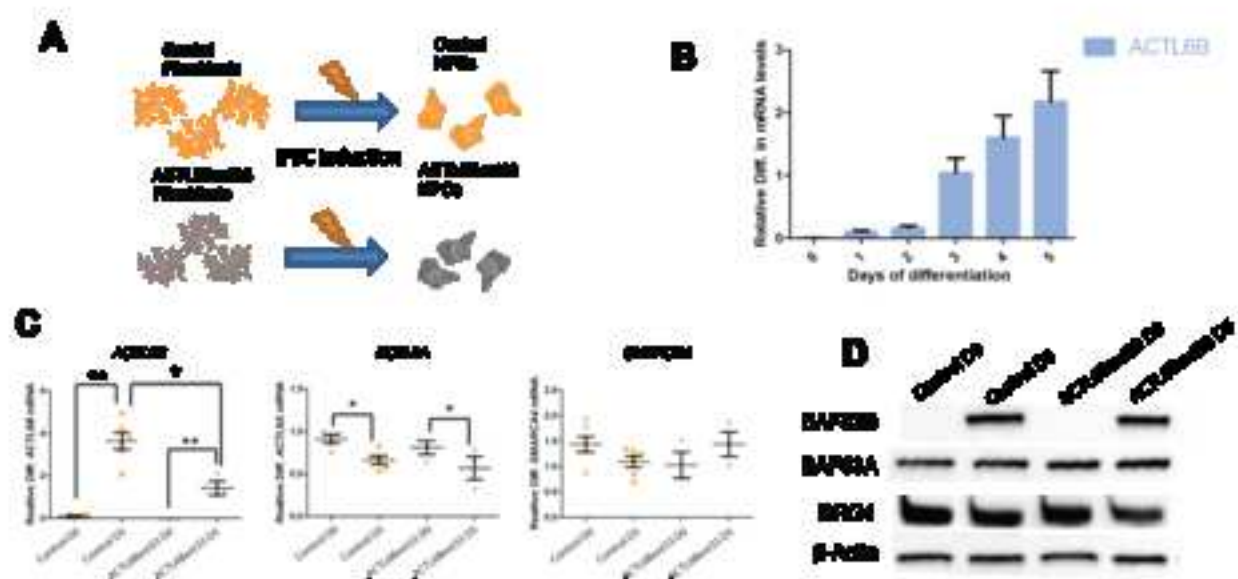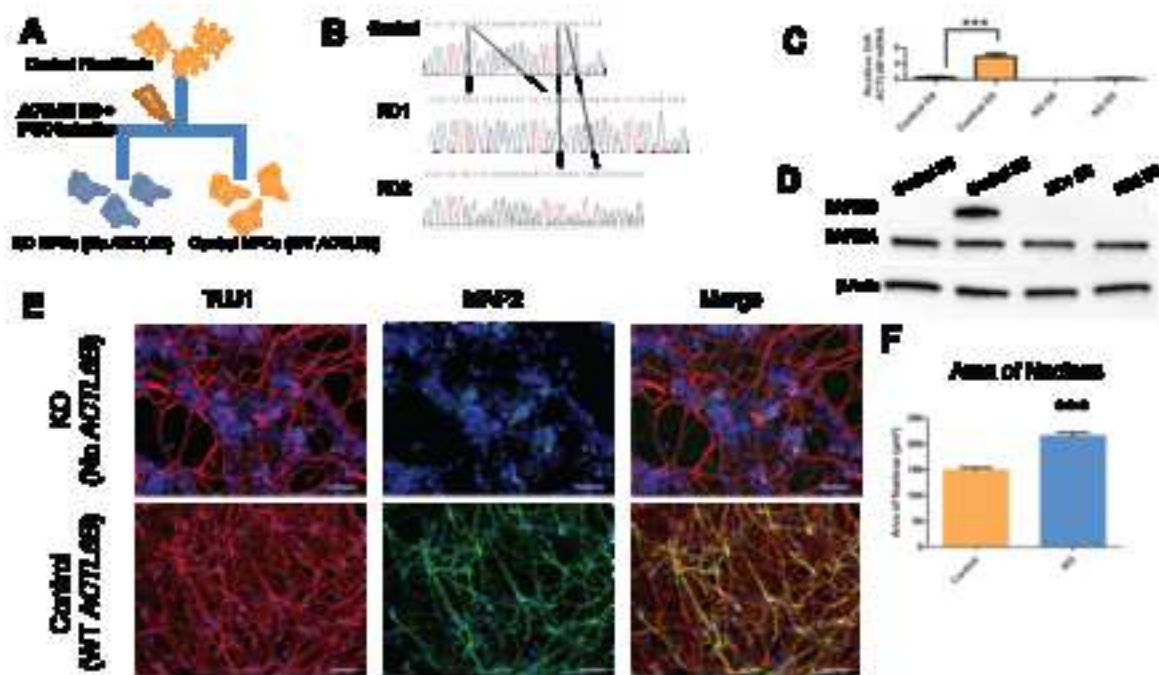1020   Nagamani, S.C.S., Cheung, S.W., Campeau, P.M., Prasad, C., et al. (2018). BAFopathies'

1021   DNA methylation epi-signatures demonstrate diagnostic utility and functional
1022   continuum of Coffin–Siris and Nicolaides–Baraitser syndromes. Nature
1023   Communications 9, 4885.
1024 34. Bogershausen, N., and Wollnik, B. (2018). Mutational Landscapes and Phenotypic
1025   Spectrum of SWI/SNF-Related Intellectual Disability Disorders. Front Mol Neurosci
1026   11, 252.
1027 35. Mari, F., Marozza, A., Mencarelli, M.A., Lo Rizzo, C., Fallerini, C., Dosa, L., Di Marco, C.,
1028   Carignani, G., Baldassarri, M., Cianci, P., et al. (2015). Coffin-Siris and Nicolaides-
1029   Baraitser syndromes are a common well recognizable cause of intellectual disability.
1030   Brain and Development 37, 527-536.
1031 36. Pretegiani, E., Mari, F., Renieri, A., Penco, S., and Dotti, M.T. (2016). Nicolaides-Baraitser
1032   syndrome: defining a phenotype. J Neurol 263, 1659-1660.
1033 37. Kosho, T., Miyake, N., and Carey, J.C. (2014). Coffin-Siris syndrome and related disorders
1034   involving components of the BAF (mSWI/SNF) complex: historical review and
1035   recent advances using next generation sequencing. Am J Med Genet C Semin Med
1036   Genet 166c, 241-251.
1037 38. Bender, H.A., Zaroff, C.M., Karantzoulis, S., Nakhutina, L., MacAllister, W.S., and Luciano,
1038   D. (2011). Cognitive and behavioral functioning in Coffin-Siris syndrome and
1039   epilepsy: a case presentation. The Journal of genetic psychology 172, 56-66.
1040 39. Santen, G.W., Aten, E., Sun, Y., Almomani, R., Gilissen, C., Nielsen, M., Kant, S.G., Snoeck,
1041   I.N., Peeters, E.A., Hilhorst-Hofstee, Y., et al. (2012). Mutations in SWI/SNF
1042   chromatin remodeling complex gene ARID1B cause Coffin-Siris syndrome. Nat Genet
1043   44, 379-380.
1044 40. Vogel-Ciernia, A., and Wood, M.A. (2014). Neuron-specific chromatin remodeling: a
1045   missing link in epigenetic mechanisms underlying synaptic plasticity, memory, and
1046   intellectual disability disorders. Neuropharmacology 80, 18-27.
1047 41. Wu, S., Shi, Y., Mulligan, P., Gay, F., Landry, J., Liu, H., Lu, J., Qi, H.H., Wang, W., Nickoloff,
1048   J.A., et al. (2007). A YY1-INO80 complex regulates genomic stability through
1049   homologous recombination-based repair. Nature structural & molecular biology 14,
1050   1165-1172.
1051 42. Vogel-Ciernia, A., Matheos, D.P., Barrett, R.M., Kramar, E.A., Azzawi, S., Chen, Y., Magnan,
1052   C.N., Zeller, M., Sylvain, A., Haettig, J., et al. (2013). The neuron-specific chromatin
1053   regulatory subunit BAF53b is necessary for synaptic plasticity and memory. Nat
1054   Neurosci 16, 552-561.
1055 43. Laeremans, A., Van de Plas, B., Clerens, S., Van den Bergh, G., Arckens, L., and Hu, T.-T.
1056   (2013). Protein Expression Dynamics During Postnatal Mouse Brain Development.
1057   Journal of Experimental Neuroscience 7, 61-74.
1058 44. Son, E.Y., and Crabtree, G.R. (2014). The role of BAF (mSWI/SNF) complexes in
1059   mammalian neural development. American journal of medical genetics Part C,
1060   Seminars in medical genetics 0, 333-349.
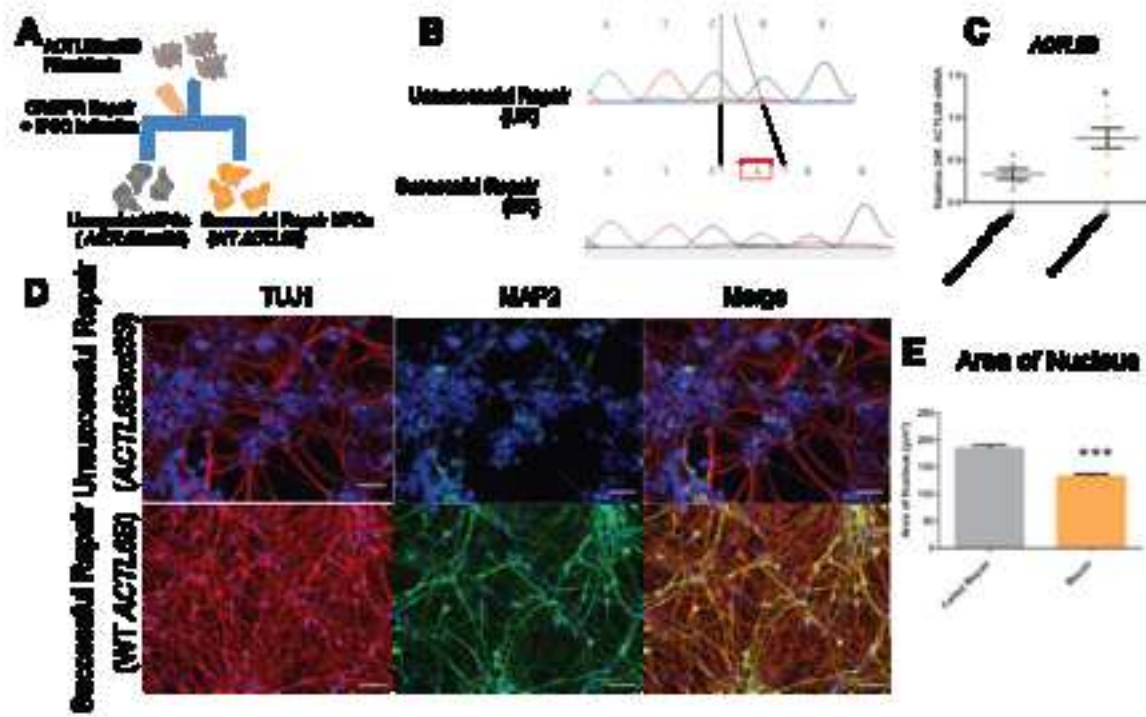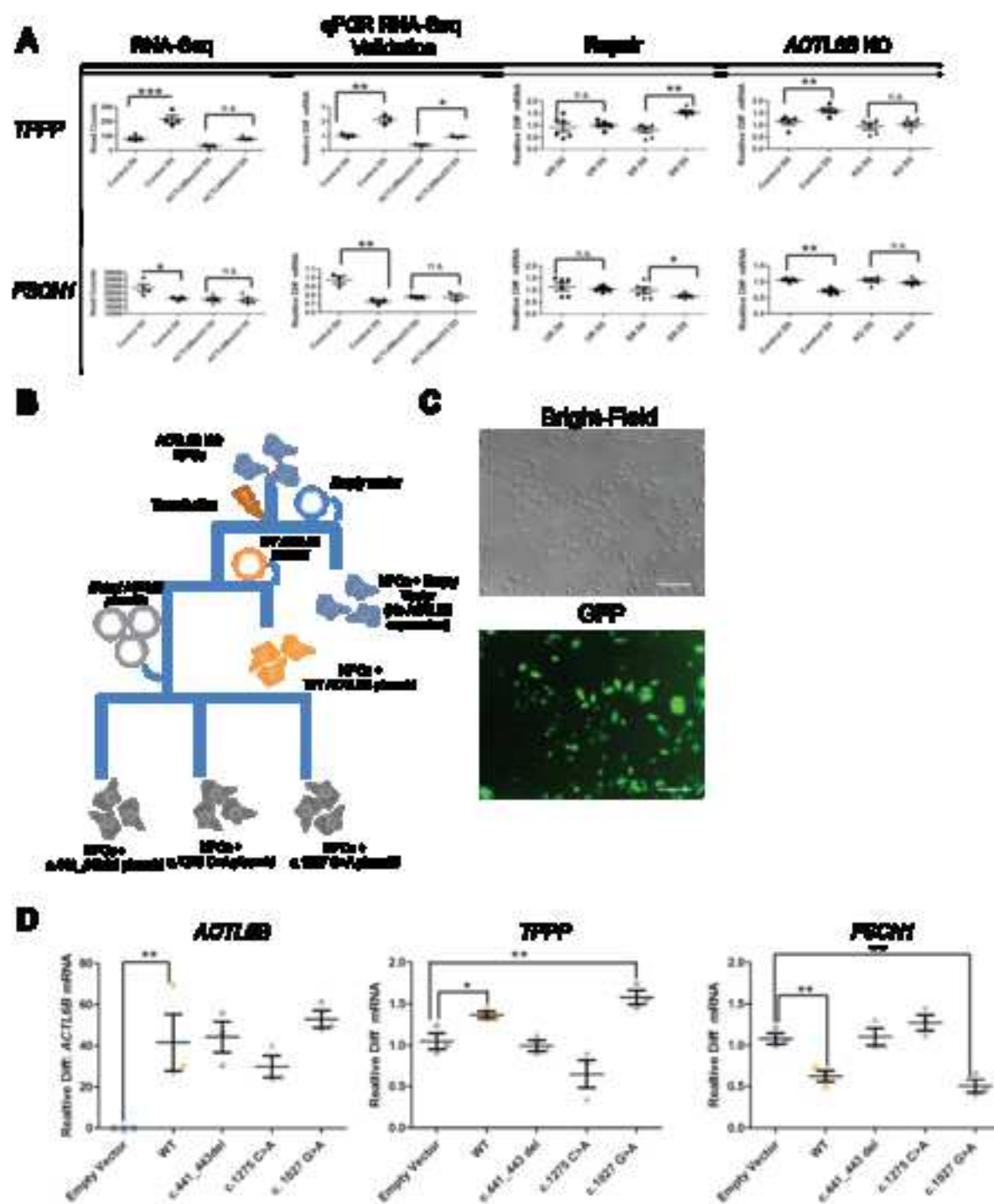
1061

Figure 1

Click here to access/download;Figure;Figure 1.png

Figure 1

Figure 2　　　　　　　　　　　　　　　　　Click here to access/download;Figure;Figure 2.png ±

A — SSEA, OCT4, Merge; TRA-1-60, NANOG, Merge

B — Nestin, SOX1, Merge; OCT4, PAX6, Merge

C — TUJ1/MAP2/DAPI

D — 20 pA

E

F

Figure 5

Click here to access/download;Figure;Figure 5.png ⬇

Figure 6

Figure 8

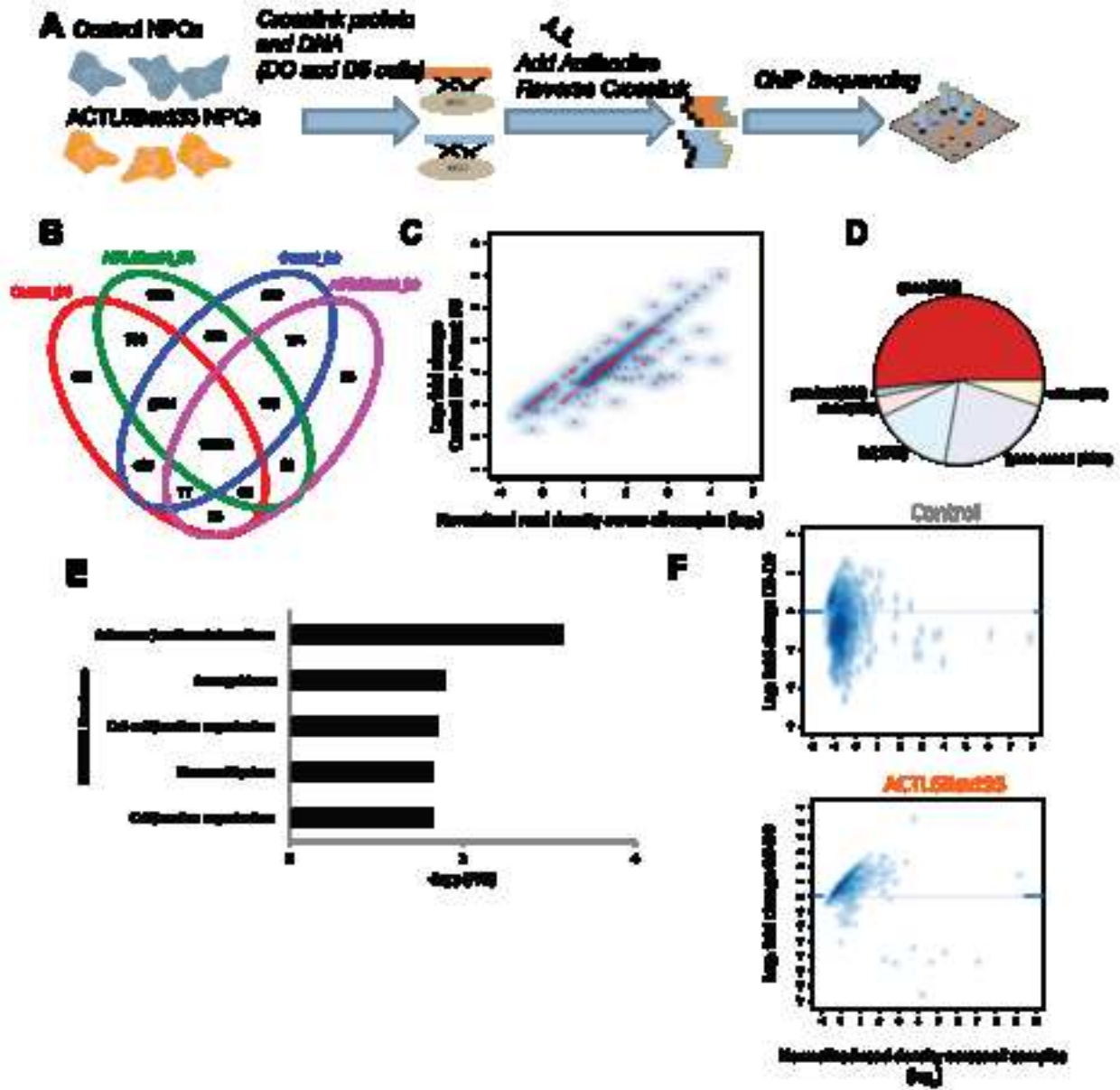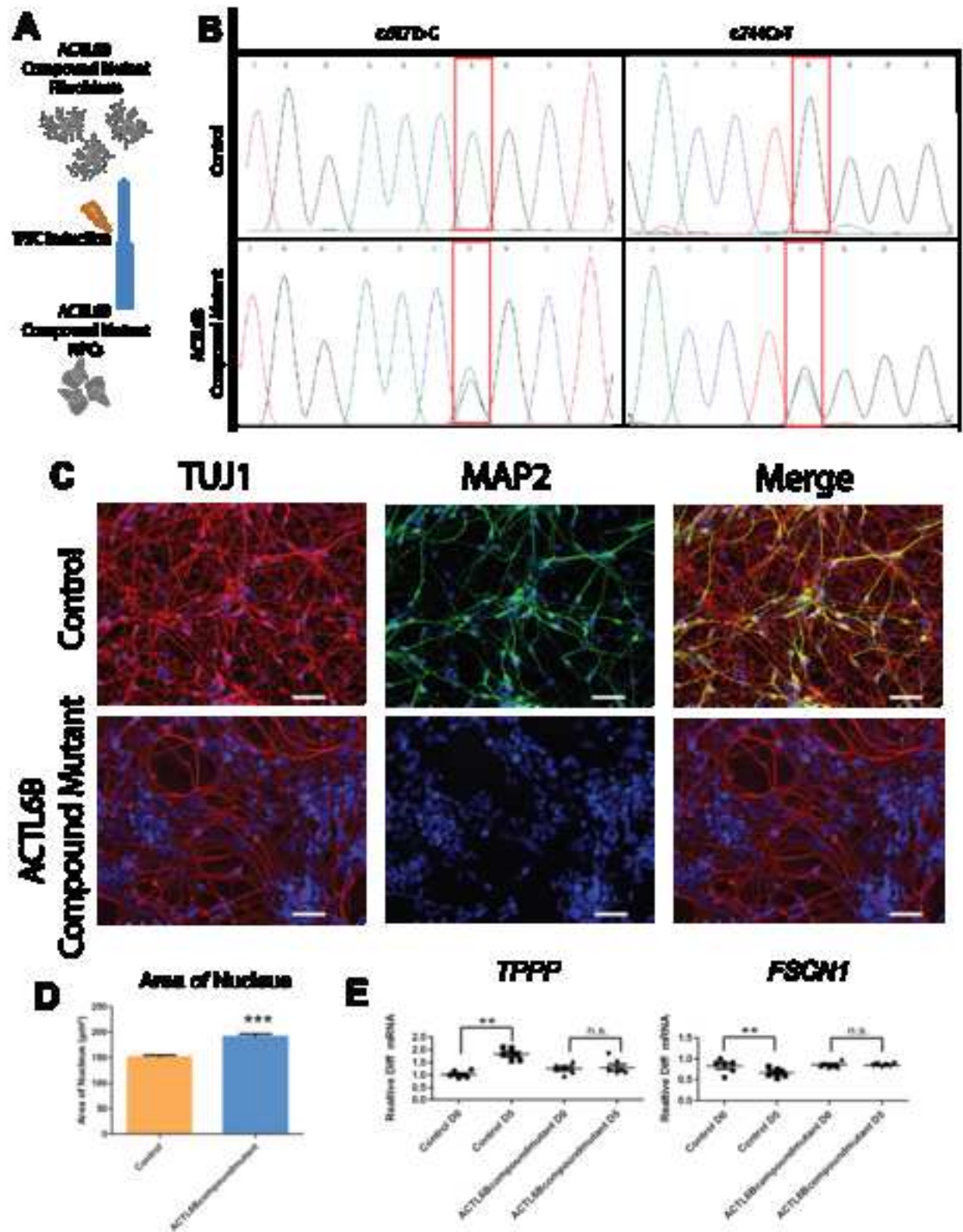Click here to access/download;Figure;Updated Figure 8.png ±

Click here to access/download

Supplemental Text and Figures

Supplementary Figures, Tables and Methods Feb 26th.pdf